



**HAL**  
open science

# The origin and collapse of rock glaciers during the Bølling-Allerød interstadial: A new study case from the Cantabrian Mountains (Spain)

Javier Santos-González, Rosa Blanca González-Gutiérrez, José María Redondo-Vega, Amelia Gómez-Villar, Vincent Jomelli, José M. Fernández-Fernández, Nuria Andrés, José M. García-Ruiz, Sergio Alberto Peña-Pérez, Adrián Melón-Nava, et al.

## ► To cite this version:

Javier Santos-González, Rosa Blanca González-Gutiérrez, José María Redondo-Vega, Amelia Gómez-Villar, Vincent Jomelli, et al.. The origin and collapse of rock glaciers during the Bølling-Allerød interstadial: A new study case from the Cantabrian Mountains (Spain). *Geomorphology*, 2022, 401, 10.1016/j.geomorph.2022.108112 . insu-03661020

**HAL Id: insu-03661020**

**<https://insu.hal.science/insu-03661020>**

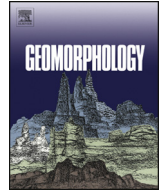
Submitted on 6 May 2022

**HAL** is a multi-disciplinary open access archive for the deposit and dissemination of scientific research documents, whether they are published or not. The documents may come from teaching and research institutions in France or abroad, or from public or private research centers.

L'archive ouverte pluridisciplinaire **HAL**, est destinée au dépôt et à la diffusion de documents scientifiques de niveau recherche, publiés ou non, émanant des établissements d'enseignement et de recherche français ou étrangers, des laboratoires publics ou privés.



Distributed under a Creative Commons Attribution 4.0 International License



## The origin and collapse of rock glaciers during the Bølling-Allerød interstadial: A new study case from the Cantabrian Mountains (Spain)

Javier Santos-González<sup>a,\*</sup>, Rosa Blanca González-Gutiérrez<sup>a</sup>, José María Redondo-Vega<sup>a</sup>, Amelia Gómez-Villar<sup>a</sup>, Vincent Jomelli<sup>b</sup>, José M. Fernández-Fernández<sup>c,d</sup>, Nuria Andrés<sup>d</sup>, José M. García-Ruiz<sup>e</sup>, Sergio Alberto Peña-Pérez<sup>a</sup>, Adrián Melón-Nava<sup>a</sup>, Marc Oliva<sup>f</sup>, Javier Álvarez-Martínez<sup>g</sup>, Joanna Charton<sup>b</sup>, ASTER Team<sup>b</sup>, David Palacios<sup>d</sup>

<sup>a</sup> Department of Geography and Geology, Universidad de León, Campus de Vegazana s/n, 24071 León, Spain

<sup>b</sup> Aix-Marseille Université, CNRS, IRD, Coll. France, INRAE, UM 34 CEREGE, 13545 Aix-en-Provence, France

<sup>c</sup> Instituto de Geografia e Ordenamento do Território (IGOT), Universidade de Lisboa, R. Branca Edmée Marques, 1600-276 Lisbon, Portugal

<sup>d</sup> High Mountain Physical Geography Research Group, Department of Geography, Universidad Complutense de Madrid, 28040 Madrid, Spain

<sup>e</sup> Instituto Pirenaico de Ecología (IPE-CSIC), Campus de Aula Dei, P.O. Box 13.034, 50080 Zaragoza, Spain

<sup>f</sup> Department of Geography, Universitat de Barcelona, C/ Montalegre, 6-8, 08001 Barcelona, Spain

<sup>g</sup> Department of Agricultural and Forest Engineering, Universidad de Valladolid, Campus La Yutera, 34071 Palencia, Spain

### ARTICLE INFO

#### Article history:

Received 3 October 2021

Received in revised form 12 January 2022

Accepted 12 January 2022

Available online 19 January 2022

#### Keywords:

Rock glacier

Deglaciation

Paraglacial processes

Cosmic-Ray Exposure dating

Bølling-Allerød interstadial

Cantabrian Mountains

### ABSTRACT

During the Late Pleistocene, the main mountain ranges of the Iberian Peninsula were covered by small icefields and cirque and alpine glaciers. The deglaciation triggered paraglacial processes that generated landforms, mostly within the ice-free glacial cirques. In this research we analyse the deglaciation process in the Muxivén Cirque (42°15'N – 6°16'W), in the upper Sil River Basin, which includes some of the largest relict rock glaciers of the Cantabrian Mountains. We addressed this objective by means of accurate geomorphological reconstructions, sedimentological analysis, Schmidt-hammer surface weathering measurements and a dataset of 10<sup>10</sup>Be Cosmic-Ray Exposure ages. Results reveal that after ~16 ka, glaciers retreated to the bottom of the cirques at the headwaters of the valley, leaving the walls free of ice and triggering rock avalanches onto the remnants of these glaciers. This paraglacial process supplied debris to a small glacier within Muxivén Cirque, which transformed in two rock glaciers. These debris isolated the ice inside the rock glaciers only for a very short period of time and ended up melting completely before the Younger Dryas. The lower sector of the largest one stabilized at 14.5 ± 1.5 ka, while the upper sector remained active until 13.5 ± 0.8 ka. Previous to the stabilization of the lower sector of the northern rock glacier, at its margin a high-energy debris avalanche occurred at ~14.0 ± 0.9 ka. These data agree with previous research, corroborating the paraglacial origin of most Iberian rock glaciers during the Bølling-Allerød interstadial.

© 2022 The Author(s). Published by Elsevier B.V. This is an open access article under the CC BY-NC-ND license (<http://creativecommons.org/licenses/by-nc-nd/4.0/>).

### 1. Introduction

Deglaciating landscapes in mountain areas and the polar regions favour the development of permafrost-related landforms, such as rock glaciers, which are thus considered the best geoindicators of permafrost in low- and mid-latitude mountain environments (Oliva et al., 2018). Indeed, there is wide consensus that rock glaciers reflect to some extent major climatic features, as they indicate the occurrence of permafrost and a mean annual air temperature (MAAT) ≤ −2 °C in the region by the time when they were active (e.g. Haeberli, 1985; Giraudi and

Frezzotti, 1997; French, 2017). However, present-day observations on how rock glaciers react to climate warming are complex and still being debated depending on latitude, altitude and aspect. In fact, MAAT increases can provoke either the acceleration of the movement of the rock glacier (Delaloye et al., 2010; Kellerer-Pirklbauer, 2012; Kellerer-Pirklbauer and Kaufmann, 2012; Wirz et al., 2016; Kellerer-Pirklbauer et al., 2017; Eriksen et al., 2018; Kenner, 2019) or, conversely, enhance its subsidence and gradual stabilization (Gómez-Ortiz et al., 2014) prior to their definitive stagnation (Emmer et al., 2015; Campos et al., 2019; Tanarro et al., 2019; Fernández-Fernández et al., 2020; Palacios et al., 2021). Moreover, rock glacier dynamics are not only driven by climate fluctuations, but also modulated by the intensity of the processes occurring on the cirque walls where micro-climatic and geomorphic processes can evolve in a different way than the regional

\* Corresponding author.

E-mail address: [jsango@unileon.es](mailto:jsango@unileon.es) (J. Santos-González).

climate (Humlum, 2000; Kirkbride, 2000; Brenning, 2005; Azócar and Brenning, 2010; Deline et al., 2015; Anderson and Anderson, 2016; Mayr and Hagg, 2019).

The use of relict rock glaciers as palaeoclimatic indicators is a complex issue due to the problems posed by the interpretation of the numerical dates obtained by different dating techniques. Nowadays, the most precise –and most commonly used– method for dating relict rock glaciers is the Cosmic-Ray Exposure (CRE) dating (Hippolyte et al., 2009; Deline et al., 2015; Moran et al., 2016; Palacios et al., 2016, 2017, 2020; Fernández-Fernández et al., 2017; Crump et al., 2017; Dede et al., 2017; Oliva et al., 2018; Winkler and Lambiel, 2018; Amschwand et al., 2021; Jomelli et al., 2020; Linge et al., 2020; Steinemann et al., 2020; Charton et al., 2021). However, there is still an active scientific debate on the significance of the CRE ages obtained from boulders of a rock glacier. Many observations indicate that the CRE ages of rock glaciers are indicative of absence of flow and not the final stabilization by complete melting of the internal ice body (Mackay and Marchant, 2016; Amschwand et al., 2021; Fernández-Fernández et al., 2020; Scherler and Egholm, 2020; Palacios et al., 2021). In any case, the total melting of core-ice and stabilization age of a rock glacier can only be determined if a large number of CRE samples are taken and an accurate understanding of the geomorphological setting is accomplished (Moran et al., 2016; Crump et al., 2017; Charton et al., 2021).

In the Cantabrian Mountains (northern Iberian Peninsula) there are no longer active rock glaciers, but those in relict state are widespread along the range, where more than 250 features have been identified (Gómez-Villar et al., 2011; González-Gutiérrez et al., 2019). Nonetheless, their age of stabilization and whether they represent a climatic phase within the complex climatic evolution of the Late Pleistocene still remains unknown (Redondo-Vega et al., 2010; Gómez-Villar et al., 2011; Pellitero et al., 2011). The roots of the rock glaciers in the Cantabrian Mountains are mostly located above 1500 m a.s.l., at the foot of quartzite or sandstone walls, being rare in other lithologies. The vast majority are N- or NE-oriented and rock glaciers exposed to the SE to WSW are very scarce (Redondo-Vega et al., 2010; Gómez-Villar et al., 2011). In general, they show a very-well preserved ridge-furrow morphology (e.g. González-Gutiérrez et al., 2019). Almost all these rock glaciers are found in glacial cirques, which suggests their origin related to the interaction between the deglaciation and the subsequent paraglacial processes (Santos-González et al., 2018). In the Cantabrian Mountains, some authors associated the rock glaciers located at different altitudes to different chronological stages (Pellitero et al., 2011; Serrano et al., 2013), but most of the studies proposed a Late Pleistocene age for all of these rock glaciers, either in the Younger Dryas stadial (YD) (GS-1; 12.9–11.7 ka) (Serrano et al., 2015) or in the Bølling–Allerød (B-A) (GI-1; 14.6–12.9 ka) interstadial (Rodríguez-Rodríguez et al., 2016, 2017). However, an accurate chronology is only available for two rock glaciers in the Cantabrian Mountains dated through CRE ( $^{10}\text{Be}$  cosmionuclide) (Rodríguez-Rodríguez et al., 2016, 2017). One is located in the headwaters of the Porma River, at the southern face of the range, with an ENE orientation and a mean stabilization age at its front (1620 m a.s.l.) of  $15.7 \pm 0.8$  ka ( $n = 5$ ; ranging from 16.6 to 15.5 ka). The other is located at the northern face of the mountains, in the headwaters of the Monasterio River. It is north-oriented, and yielded a mean age of  $13.0 \pm 0.5$  ka ( $n = 5$ ; from 13.7 to 12.4 ka) in its front (1540 m a.s.l.). The origin of these rock glaciers has been interpreted as the terminal stage of the shrinking Late Pleistocene glaciers that occurred during the B-A interstadial. The CRE age differences in both rock glaciers provide evidence of the importance of the topography controlling their dynamics, with slightly younger ages in the less favourable aspects (Rodríguez-Rodríguez et al., 2017).

The results recorded for the rock glaciers stabilization in the Cantabrian Mountains are similar to those obtained in other relict rock glaciers throughout the Iberian Peninsula (Oliva et al., 2019). The vast majority of the alpine cirques in Iberian mountains below 2800 m a.s.l.

were deglaciated shortly before or during the B-A interstadial, by  $15.1 \pm 1.3$  ka (mean age;  $n = 21$ ; ranging from  $16.3 \pm 3.3$  ka to  $13.2 \pm 0.7$  ka; Palacios et al., 2020), when MAAT values were similar to present-day according to marine and terrestrial records (Fletcher et al., 2010a, 2010b; Moreno et al., 2014; Rasmussen et al., 2014; López-Sáez et al., 2020; Bernal-Wormull et al., 2021). In many of these cirques, rock glaciers formed shortly after the deglaciation and their fronts became inactive or stabilized within the same interstadial, as it has been reported from the Central (Palacios et al., 2017; Oliva et al., 2021) and Eastern Pyrenees (Andrés et al., 2018), the Iberian Range (García-Ruiz et al., 2020), the Central Range (Palacios et al., 2012), and the Sierra Nevada (Palacios et al., 2016, 2019). On the few cases where boulders from the upper sectors of relict rock glaciers in the Iberian Peninsula have been dated, data confirmed that these features remained active for much longer and only became inactive or stabilized during the mid-Holocene, often during the Holocene Thermal Maximum (HTM; 11–5 ka BP; Renssen et al., 2012) (Palacios et al., 2016, 2017, 2020; Fernández-Fernández et al., 2017; Andrés et al., 2018; Oliva et al., 2021).

Despite these recent advances in the knowledge of the age of the rock glaciers in the Iberian mountains, there still remain major uncertainties about their geomorphological and palaeoclimatic meaning as inactive landforms, methodological issues inherent to the CRE dating. In this work, we will approach these gaps by addressing the following specific questions:

- (i) What is the geomorphological meaning of the CRE ages obtained from surface boulders of the rock glaciers? To date, it is still not clear whether they represent the age of the definitive stabilization of the rock glacier or, on the contrary, they indicate a previous period of limited and slow flow towards an inactive state and the complete disappearance of the inner ice.
- (ii) What is the palaeoclimatic significance of these formations? The current knowledge is uncertain about (i) if the development of the currently relict rock glaciers was the consequence of a cold, generally dry, climatic phase with the extension of permafrost; or (ii) if they represent a warmer phase that favoured the transformation of the debris-free glaciers into rock glaciers.

These questions are addressed through a study case focuses on the Muxivén glacial Cirque, which has been selected as representative of the Cantabrian Mountains due to the wide variety of glacial, periglacial and paraglacial landforms that it hosts.

## 2. Study area

The Cantabrian Mountains are located in NW Iberian Peninsula, northern Spain. They run parallel to the Cantabrian coast for ~500 km from W to E and are ~80 to 120 km wide from N to S (Fig. 1A), with the highest altitudes ranging from 1800 to 2648 m a.s.l. At present, this range is fully deglaciated, but small ice patches and isolated permafrost exist in the highest cirques (Serrano et al., 2011; Ruiz-Fernández et al., 2016; Pisabarro et al., 2017). The relief is very steep on the northern slope due to its proximity to the Cantabrian Sea, while on the southern side the valleys are wider and located at higher altitudes.

The study area is located in the western part of the southern slope of this range, in the Sil River headwaters, which flow into the Miño River and the Atlantic Ocean (Fig. 1B). This basin shows gentle relief in the upper part, with extensive surfaces between 1500 and 2100 m, while narrow valleys prevail below this altitude. The Lumajo Valley, drained by the Almozarra River, runs 11.7 km N-S from the Cornón Peak (2188 m a.s.l.) to the Sil River (1050 m a.s.l.).

We analyse a small cirque located between the eastern slope of the Muxivén Peak (2027 m a.s.l.) and the Lumajo village (1390 m a.s.l.), at  $42^{\circ}15'N$  and  $6^{\circ}15' - 6^{\circ}16'W$  (Fig. 1C). The study area is located in the

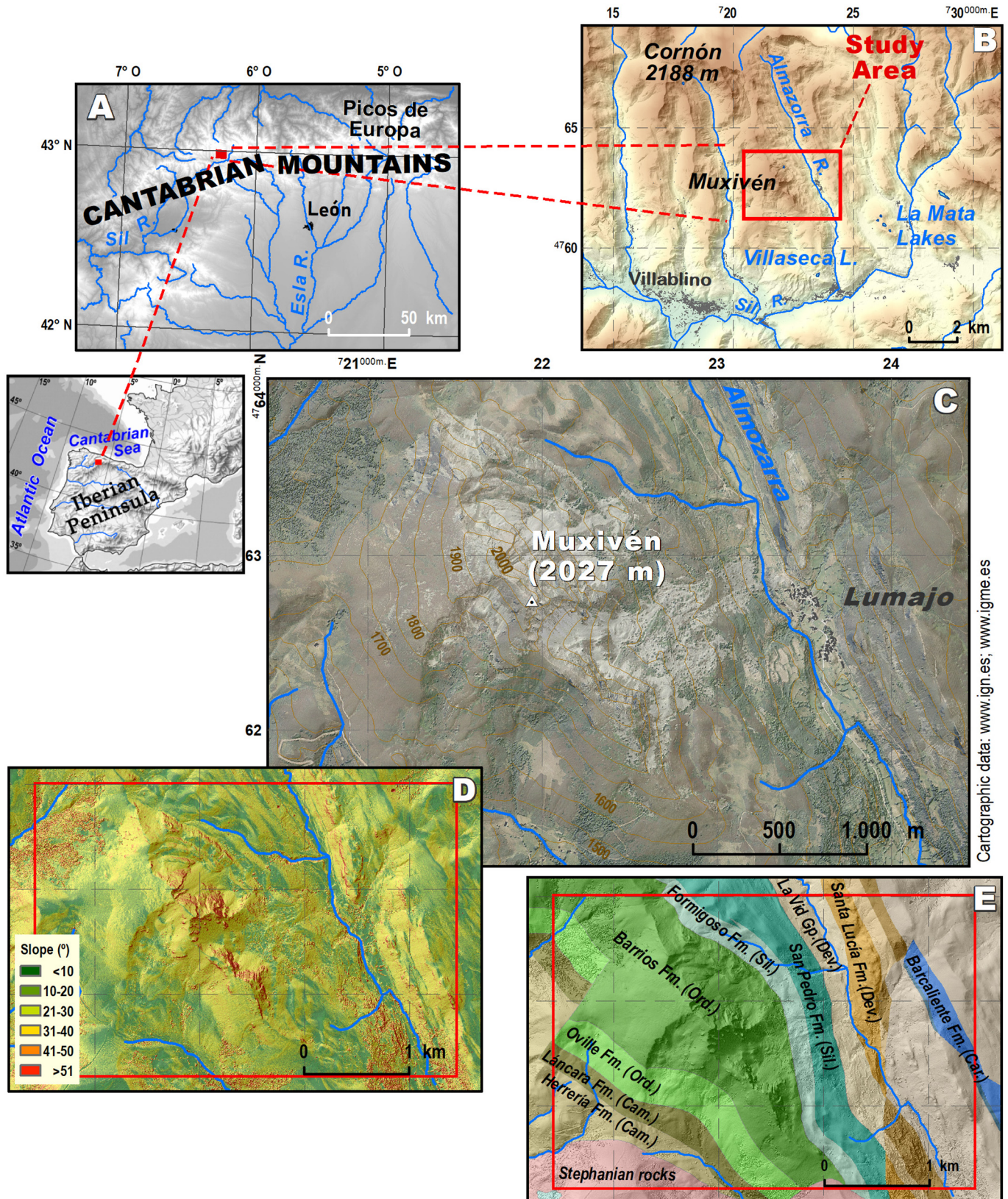


Fig. 1. Location of the study area within the Iberian Peninsula and the Cantabrian Mountains (A), and the upper Sil River Basin (B). Orthophoto and topographical map (C), together with the slope (D) and geological and lithological conditions (E) existing in the area. Cam: Cambrian. Ord: Ordovician. Sil: Silurian. Dev: Devonian. Car: Carboniferous.

geological unit of the Cantabrian Zone (Alonso et al., 2009), which is part of the Astur-Galaic region of the Alpine-Pyrenean Orogen (Martín-González and Heredia, 2011). Palaeozoic siliceous materials

are dominant. The Muxivén Cirque is composed of Ordovician white quartzites (Barrios Fm.), while Silurian black slates (Formigoso Fm.) and Silurian ferruginous sandstones (San Pedro Fm.) appear to the

east, and Devonian limestones, dolomites and slates close to Lumajo Valley (La Vid Fm.) (Fig. 1F).

The climate is oceanic with Mediterranean influence that entails a reduced summer precipitation. Annual precipitation is around 1800–2000 mm and a MAAT of  $\sim 6$  °C is recorded at 1600–1700 m, according to the nearby meteorological stations data. Snow-cover is frequent throughout the winter especially above 1700 m, with some long-lasting snow-patches persisting until late spring and early-summer.

This area was included the most extensive glacial system developed in the Cantabrian Mountains during the Late Quaternary, covering  $\sim 800$  km<sup>2</sup>, 450 of them in the Sil basin (Jiménez-Sánchez et al., 2013; Santos-González et al., 2013a, 2021; Rodríguez-Rodríguez et al., 2015; Serrano et al., 2017). The lowest glacial deposits in this catchment are located at 750 m, i.e. 52 km downstream from the headwaters (Santos-González et al., 2013b). The Lumajo Valley was part of the transfluent and icefield glaciers of the upper Sil palaeoglacier, where few palaeonunataks, such as the Muxivén Peak, stand out (García de Celis and Martínez Fernández, 2002; Alonso and Suárez Rodríguez, 2004; Jalut et al., 2004, 2010; Santos-González et al., 2013a, 2021). The ice thickness exceeded 350 m. <sup>14</sup>C dates in Villaseca and La Mata lakes, in the lower part of the Lumajo Valley (Fig. 1B), revealed that glacier recession from the local glacial maximum started between 44 and 35 cal ka BP (Jalut et al., 2004, 2010). The same authors pointed out that the final deglaciation in main valleys probably occurred around 16 cal ka BP (Jalut et al., 2010).

Following the glacier retreat, rock glaciers formed on the eastern slope of the Muxivén Peak (Gómez-Villar et al., 2011). Vidal Box (1958) was the first author who described the glacial morphology, the rocky deposits and the geology of the Lumajo Valley and the Muxivén Peak. However, the first reference to the existence of a rock glacier was made by García de Celis (1997), who pointed out its geographical extent and major characteristics. Jalut et al. (2004, 2010) reconstructed glacial dynamics from the lacustrine deposits in the Villaseca and La Mata lakes, in the Lumajo and Sil valleys respectively, very close to the Muxivén Peak. They proposed that glacial retreat in Lumajo valley took place at  $\sim 16$  cal ka BP, although they did not analyse the subsequent geomorphological evolution.

Due to the large size and complex development of the rock glaciers at the foot of the Muxivén Peak in comparison with other landforms in this range (Redondo-Vega et al., 2004; Gómez-Villar et al., 2011), they were included as geomorphosites in the inventory of the Alto Sil Natural Area (Santos-González and Redondo-Vega, 2006), and some years later in the Lumajo Valley geosite, in the geosites inventory of the León Province (Fernández Martínez et al., 2009). Therefore, it is included in the viewer of the national inventory of geosites (<http://info.igme.es/ielig/>). The inclusion of these landforms has recently attracted the scientific interest for understanding their formation and subsequent landscape evolution in the area (Rodríguez et al., 2020).

### 3. Methods

#### 3.1. Geomorphology and sedimentology

A detailed geomorphological map of the Muxivén Cirque was constructed using the Geographic Information System (GIS) ArcMap 10.7 (Esri), based on extensive fieldwork, photointerpretation and previous geomorphological studies. The map has been used as a framework to place the development of the Muxivén rock glacier in a broader geomorphological context. The characterization of the different types of landslides has followed the classification of Hungr et al. (2014).

Using an unmanned aerial vehicle (UAV) we obtained an updated cartographic base from orthophotos and a Digital Surface Model (DSM) with great detail (between 6 and 20 cm resolution). The use of a DJI Phantom 4 Multispectral model, equipped with a Global Navigation Satellite System (GNSS), Real-Time Kinematic (RTK) system,

allowed achieving very accurate images thanks to this positioning system (Štroner et al., 2020). With a proper overlap configuration (75% frontal and 60% lateral) and the use of few Ground Control Points (GCP), we were able to improve small errors and distortions to ensure the highest possible accuracy (Oniga et al., 2020). The images obtained were processed through Structure from Motion (SfM) techniques, which are based on the elaboration of a 3D structure from the overlapping of all the obtained images (Westoby et al., 2012).

Boulders over 4 m long (maximum diameter) have been identified in the entire study area using different orthophotos (Spanish National Orthophoto Program orthophotos of 2017 and 2020, and the UAV-derived one), UAV oblique photographs from the different sectors and the Digital Terrain Model (DTM) at 2 m resolution obtained by the Spanish National Geographic Institute LiDAR. Such boulders were vectorized as polygon shapefiles in the GIS work environment and their axis were retrieved through the "Minimum Bounding Geometry".

Grain size analyses were also performed in the main deposits, according to geomorphological results. In each of them, we measured the three axis of 50 clasts in a representative section of the deposit. For a better interpretation of the landforms, macrofabric analysis has been performed in 10 sites including different types of deposits (rock glaciers, talus slopes and debris avalanche). Sectors with homogeneous morphology and representative of each landform have been selected for sampling. In each of them, 50 clasts exceeding 20 cm in size (Kjær and Krüger, 1998) were measured considering the main axis declination and dip for each clast, covering surfaces of 2–5 m<sup>2</sup> depending on the availability of clast. These measures were carried out using the clasts AB plane and only elongated clasts were chosen (a long / intermediate axis ratio  $>1.5$ ) with the two major axes well-defined because these clasts shape better reflect unidirectional fluxes in their transport and sedimentation (Andrews, 1971; Benn and Evans, 1996; Benn and Ringrose, 2001; Evans, 2017).

The data were plotted using the software *Orient 3* (Vollmer, 1995, 2015) and represented in a stereonet or Lambert equal-area spherical projection, using the lower hemisphere, where the area is preserved and the densities are not distorted. The data were contoured following the method of Diggle and Fisher (1985) so that areas with the same density concentration are presented. Thus, the contours show whether the fabric is isotropic (without a main direction), girdle (points distributed around a circle) or cluster (the majority of the points are grouped).

The directional data have been quantified by calculating the average values through the factorial analysis of the eigenvalues (Woodcock, 1977; Benn, 1994). Each fabric is summarized in three values, the eigenvectors ( $V_1$ ,  $V_2$  and  $V_3$ ) describing the maximum, the intermediate and the minimum preferred directions and dips in three perpendicular axes. Also, the eigenvalues ( $S_1$ ,  $S_2$  and  $S_3$ ) were identified showing the concentration degree around their respective axis. The relationship between the three eigenvalues allows the fabric shape identification in each sample: the cluster fabric ( $S_1$  is predominant), the girdle fabric (the  $S_1$  and  $S_2$  values are similar) and the isotropic shape (the three values are close to each other) (Watson, 1966; Mark, 1973; Johnson, 1990; Evans and Benn, 2004).

#### 3.2. Schmidt-hammer dating

The Schmidt-hammer has been applied to estimate the (relative) exposure time of rock glacier boulder surfaces, through weathering measurements with a scale up to 100 of the rebound value (Goudie, 2006), which helps to differentiate relative chronological stages. Hence, when combined with other dating techniques, it is possible to establish a Schmidt hammer-derived chronology (e.g. Tomkins et al., 2018a, 2018b, 2021; Winkler and Lambiel, 2018; Marr et al., 2019; Matthews et al., 2019; Winkler et al., 2020).

We measured Schmidt-hammer rebound (SH-R) values using the electronic Proceq® RockSchmidt (Type N), with an impact energy of 2.207 Nm for its plunger. A total of 14 sites (84 boulders) were selected

covering different geomorphological contexts from 1380 to 1735 m a.s.l. and including different coarse periglacial and slope deposits. We select the locally higher parts of the deposits (i.e. ridges) in order to minimize the possible snow influence (Ballantyne et al., 1990). Only boulders over 50 cm in the long axe (most of them between 100 and 200 cm) and in stable and prominent locations were chosen. In each boulder, we restricted the impacts to flat surfaces on lichen-free quartzite, considered to be the most reliable areas (Guglielmin et al., 2012). Boulders with visible cracks or weaknesses were avoided.

There is no agreement on the recommended number of impacts between researchers. Some authors recommended select the upper values. For example, the International Society for Rock Mechanics (1978) recommends the upper 10 values of 20 rebound values. The low impact values usually reflect 'that the rock was weakened by the actual impact of the hammer on the rock surface, or to small rock flaws that were not spotted visually before the impact was applied' (Goudie, 2006). For that reason, we test all boulders with previous impacts in some areas to find the best location. This procedure could reduce the sample size necessary to have enough statistical significance (Niedzielski et al., 2009). In each site we performed 72 impacts, spread over six boulders with 12 impacts on each one, discarding the two lowest values, using a total of 60 impacts in each site.

Data collection was introduced in a spreadsheet where the mean values and their 95% confidence intervals were calculated, and then, the data of each boulder was represented through box-plots including the mean value of each location.

### 3.3. Sample collection, processing and exposure age calculation

We collected 10 samples for CRE dating by means of a hammer and a chisel following the procedures outlined at Gosse and Phillips (2001). We targeted boulders belonging to the rock glacier and the derived debris avalanche, according to geomorphological results. As a reliability criterion for sampling in the rock glacier, we preferred well-anchored boulders and far from the rock walls so that the risk of sampling rock fall boulders is minimized. Also, aiming to avoid the problems typically associated to the topographic and snow shielding and to optimize the cosmic-ray flux reception: (i) we preferred boulders located at the top of the ridges from which the snow is expected to be easily blown away; and (ii) we sampled flat-topped and gentle-sloping surfaces (<35°). The thickness of the extracted samples ranged from 1.5 to 7 cm (Table 1). In addition, in order to account for any partial shielding due to the surrounding topography, we calculated the topographic shielding factor for every sampling site through the ArcGIS toolbox designed by Li (2018), which implements well-known routines explained in Dunne et al. (1999); it only requires a point shapefile of the sample

locations including the strike and the dip of the sampling surfaces, and a digital elevation model from which the skyline is created.

Before conducting the chemical processing of the samples, they were crushed and sieved to the 0.25–0.8 mm fraction at the 'Physical Geography Laboratory' of the Universidad Complutense de Madrid (Spain). Following this initial stage, we processed the rock samples at the 'Laboratoire National des Nucléides Cosmogéniques' (LN<sub>2</sub>C) of the 'Centre Européen de Recherche et d'Enseignement des Géosciences de l'Environnement' (CEREGE; Aix-en-Provence, France). According to the quartz-rich lithology of the samples, i.e. quartzite, they were processed for the extraction of the in situ-produced cosmogenic nuclide beryllium-10 (hereafter <sup>10</sup>Be).

Aiming to remove magnetic minerals, samples passed through a 'Frantz LB-1' magnetic separator. Once the non-magnetic fraction was concentrated, it underwent several chemical attacks with a concentrated mixture of hydrochloric (HCl; 1:3) and hexafluorosilicic (H<sub>2</sub>SiF<sub>6</sub>; 2:3) acids to dissolve and discard the non-quartz minerals (e.g. feldspars). Subsequently, some successive partial dissolutions of the remaining minerals with concentrated hydrofluoric acid (HF) helped to dissolve the remaining impurities (e.g. non-dissolved feldspar minerals) and to decontaminate the quartz from atmospheric <sup>10</sup>Be. These procedures resulted in pure quartz masses ranging from 8 to 20 g (Table 4).

Just before the total dissolution of quartz, ~150 µL of an in-house manufactured (from a phenakite crystal) <sup>9</sup>Be carrier solution (spike, concentration: 3025 ± 9 µg g<sup>-1</sup>; Merchel et al., 2008) were added to the samples. The purified quartz was subsequently dissolved by acid leaching with 48% concentrated HF (3.6 mL per g of quartz + 30 mL in excess). The Be samples were then precipitated to beryllium hydroxide (Be(OH)<sub>2</sub>) at pH = 8 by means of ammonia (NH<sub>3</sub>). Subsequently, Be was separated from other elements through resin columns: a Dowex 1 × 8 anionic exchange column was used to remove elements such as Fe, Mn and Ti, while a Dowex 50WX8 cationic exchange column was used after that aiming to discard B and recover Be (Merchel and Herpers, 1999). Following the final elution, Be was precipitated again, dried and oxidized to BeO at 700 °C. Finally, the targets for accelerator mass spectrometer (AMS) measurements were prepared by mixing the BeO with niobium powder keeping an approximate 1:1 proportion, and the mixture was pressed into copper cathodes.

The targets were analysed at the 'Accélérateur pour les Sciences de la Terre, Environnement et Risques' (ASTER) French national AMS facility at CEREGE in order to measure the <sup>10</sup>Be/<sup>9</sup>Be ratio from which the <sup>10</sup>Be concentration was later inferred (Table 2). The AMS measurements were calibrated against the in-house standard STD-11 with an assigned <sup>10</sup>Be/<sup>9</sup>Be ratio of (1.191 ± 0.013) × 10<sup>-11</sup> (Braucher et al., 2015). Analytical 1σ uncertainties include uncertainties in the AMS counting

**Table 1**  
Field data of the sampling sites, topographic shielding factor, sample thickness and distance from the headwall.

Sample name	Latitude (DD)	Longitude (DD)	Elevation (m a.s.l.) <sup>a</sup>	Map and ground distance from the headwall (m)	Topographic shielding factor	Thickness (cm)
Upper northern rock glacier						
MUX-1	42.9834	-6.2715	1669	534 (1038)	0.9644	3.5
MUX-2	42.9833	-6.2714	1668	544 (1051)	0.9542	4.0
MUX-3	42.9832	-6.2713	1667	555 (1060)	0.9658	5.5
Lower northern rock glacier						
MUX-4	42.9844	-6.2665	1559	921 (1541)	0.9891	3.2
MUX-5	42.9844	-6.2665	1559	924 (1544)	0.9891	3.1
MUX-6	42.9842	-6.2668	1563	899 (1515)	0.9879	1.5
Debris avalanche						
MUX-7	42.9857	-6.2605	1402	1409 (2217)	0.9868	2.1
MUX-8	42.9857	-6.2605	1401	1409 (2217)	0.9868	4.0
MUX-9	42.9857	-6.2605	1401	1409 (2217)	0.9854	6.9
MUX-10	42.9856	-6.2607	1400	1397 (2209)	0.9869	4.6

<sup>a</sup> Elevation data were taken from the LIDAR 5 m digital elevation model produced by the Spanish 'Instituto Geográfico Nacional' (vertical accuracy of ±5 m); available online at: <http://centrodedescargas.cnig.es/CentroDescargas/index.jsp>.

**Table 2**  
Eigenvalues data of the macrofabric samples.

Samples	Orientation slope (°)	Eigenvalue 1			Eigenvalue 2			Eigenvalue 3		
		V <sub>1</sub> (°)	Dip (°)	S <sub>1</sub>	V <sub>2</sub> (°)	Dip (°)	S <sub>2</sub>	V <sub>3</sub> (°)	Dip (°)	S <sub>3</sub>
Talus slope	120	110	28	0.70	208	15	0.22	322	57	0.07
Rock fall scree	82	52	14	0.56	144	9	0.31	266	73	0.12
Upper Northern rock glacier, ridge	127	317	8	0.46	48	7	0.39	179	79	0.15
Upper Northern rock glacier, depression	132	62	23	0.72	156	8	0.20	265	65	0.09
Lower Northern rock glacier, external ridge	59	132	7	0.47	41	5	0.37	279	81	0.16
Lower Northern rock glacier, ridge	57	119	10	0.48	29	4	0.33	278	79	0.19
Lower Northern rock glacier, furrow	57	269	11	0.47	0	4	0.33	110	79	0.20
Debris avalanche, lowest part	73	29	3	0.52	297	30	0.31	123	60	0.17
Debris avalanche (opposite slope)	252	89	16	0.48	184	17	0.30	319	66	0.22

statistics and an external 0.5% AMS error (Arnold et al., 2010) and the uncertainty related to the chemical blank correction. The <sup>10</sup>Be half-life considered was  $(1.387 \pm 0.0012) \times 10^6$  years (Chmeleff et al., 2010; Korschinek et al., 2010).

We calculated <sup>10</sup>Be exposure ages by using the CREp online calculator (Martin et al., 2017; available online at: <http://crep.crp.cnr.fr/#/>), where we selected the following settings: Lal/Stone time dependent (Lal, 1991; Stone, 2000; Balco et al., 2008), scaling scheme, ERA40 atmospheric model (Uppala et al., 2005) and the geomagnetic record of Atmospheric <sup>10</sup>Be-based VDM (Muscheler et al., 2005; Valet et al., 2005). We chose the 'European mean' production rate derived from the ICE-D online calibration dataset (Martin et al., 2017; available online at: <http://calibration.ice-d.org/>), which yielded a sea level high latitude (SLHL) <sup>10</sup>Be production rate of  $4.14 \pm 0.20$  atoms g<sup>-1</sup> yr<sup>-1</sup>, a value close to the 'world' mean of  $4.09 \pm 0.19$  atoms g<sup>-1</sup> yr<sup>-1</sup>. Exposure age results of the samples are shown in Table 4, together with their full 1σ uncertainties (derived from analytical and production rate uncertainties) and their analytical uncertainties only. The uncertainties discussed throughout the text include the full error (i.e. analytical + production rate uncertainties) unless otherwise is stated. Aiming to identify potential age outliers, the chi-squared test according to Ward and Wilson (1978) was applied to the groups of samples belonging to the same geomorphological units.

Our CRE results are compared in the discussion with those obtained in other Iberian mountains in previous publications. To ensure an adequate age contrast, we have followed the results of the recalculated CRE ages in Oliva et al. (2019) with a model similar to ours, although we cite the publications from which the data originate.

## 4. Results

### 4.1. The Muxivén rock glaciers and its geomorphological context

The eastern face of the Muxivén Cirque is dominated by the presence of two rock glaciers: the northern and the southern ones. The northern shows more mature and better-preserved morphology, including two different sectors (lower and upper part), while the southern one shows less-defined morphology. Therefore, this work focused mainly on the northern rock glacier.

These rock glaciers are located in a context of varied past and current geomorphological processes and landforms, that are relevant to understand the postglacial evolution of the cirque and the genesis of the rock glaciers. Consequently, the following units were differentiated, chronostratigraphically ordered from oldest to the youngest (Fig. 2):

- (i) A short remnant of a lateral moraine ridge runs from NW to SE, descending from 1540 to 1500 m a.s.l. (Fig. 3). It is located down valley of the glacial cirque, oriented from NW to SE, and covered by dense scrub. No visible sections or large blocks were detected, but all visible (small) boulders were of quartzite lithology.
- (ii) Rock avalanche deposits, probably from polygenic origin, are located under a scar in the main cirque rock wall and reach the

bottom of the cirque, showing a chaotic morphology, without clast sorting, and includes some depressions (Fig. 4). The deposit is partially dismantled in its distal part, where it connects with other non-active landforms, particularly the rock glaciers.

- (iii) The northern rock glacier is a complex landform composed of two different sectors (Figs. 2, 3): (a) The lower part (from 1600 to 1510 m a.s.l., 400 m long and 180 m width) shows a very well-defined longitudinal and, mainly, transversal ridge-and-furrow morphology (Fig. 5C), scattered collapse depressions and sharp lateral and frontal ridges. Its southern margin is adjacent to the debris avalanche and their frontal part on a topographic threshold with a clear change in gradient. The ridges are relatively well-colonized by heather, indicating the presence of fine material underneath the superficial clast-supported deposit. (b) The upper sector (from 1685 to 1645 m a.s.l., 190 m long and 180 m width) overlaps the lower sector and the rock avalanche deposits (Fig. 4). Again, it shows a very well-defined transverse ridge-and-furrow morphology, with scattered collapse depressions and the classical steep front of rock glaciers. Vegetation is scarce in this upper sector (Fig. 5A), suggesting the predominance of a block-supported facies with poor or almost absent fine matrix.
- (iv) The front of the lower sector of the northern rock glacier surpasses the threshold of the main U-shaped valley and falls towards the valley bottom, forming a talus slope with a convex profile with no ridges or furrows and inverse grain size grading (Fig. 3) until 1370 m a.s.l.
- (v) The southern rock glacier, from 1650 to 1540 m a.s.l., is 300 m long and 170 m width and has its roots at the foot of the rock avalanche deposits (unit ii) and includes some transversal and few longitudinal ridges (and furrows) with many depressions. The morphology of this rock glacier is less defined than the northern rock glacier (i.e. less-defined transversal ridges, poor defined frontal-lateral ridges in its limits) (Fig. 3). It is composed of very big boulders, many of them higher than 4 m of long axis.
- (vi) A well-defined debris avalanche (from 1580 m to 1370 m a.s.l.), derived from the southern margin of the lower sector of the northern rock glacier. It is 650 m long but only 30–45 m wide. The deposit of this debris avalanche descended to the valley floor in parallel to the lower sector of the rock glacier and rose up the opposite slope of the main valley, leaving deposits 35 m above the present valley floor, being wider in this part (up to 80 m) (Fig. 3). It is composed of large quartzite boulders (with some >4 m of long axis) and without fine matrix (Fig. 5D).
- (vii) Rock fall screes cover the highest part of the slopes in the cirque headwall and other rocky walls (from 1950 to 1670 m a.s.l.) (Fig. 4). The foot of some of these screes form relict creep talus.

The sedimentological analysis was carried out in the two sectors of the northern rock glacier, the debris avalanche and the talus slopes (Fig. 2B), in order to establish potential geomorphic connections and temporal relationships with the rock glacier. In addition, Schmidt-

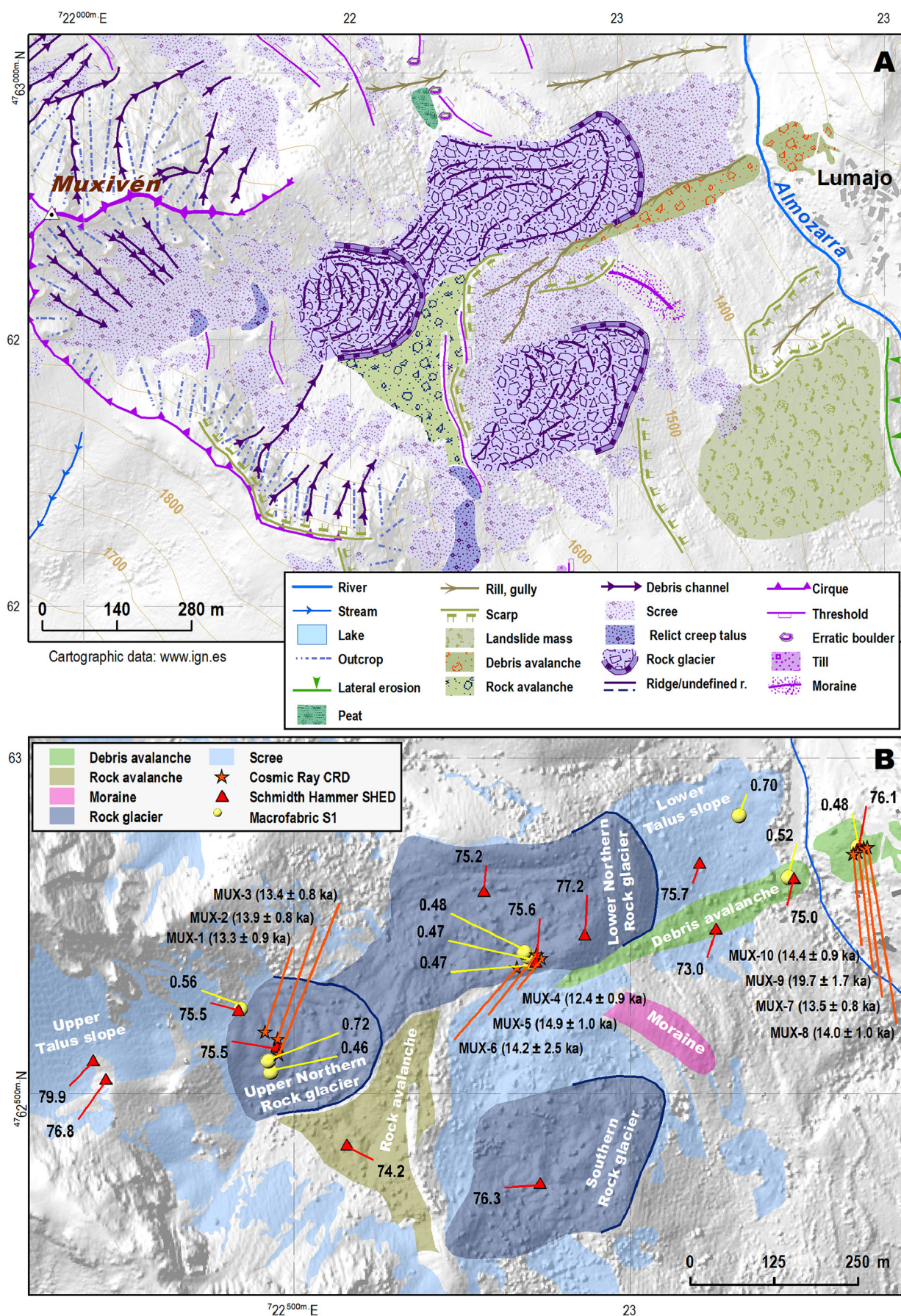


Fig. 2. Geomorphological map of the study area (A), including samples location and Cosmic-ray, Schmidt-hammer and macrofabric (S<sub>1</sub>) data (B).

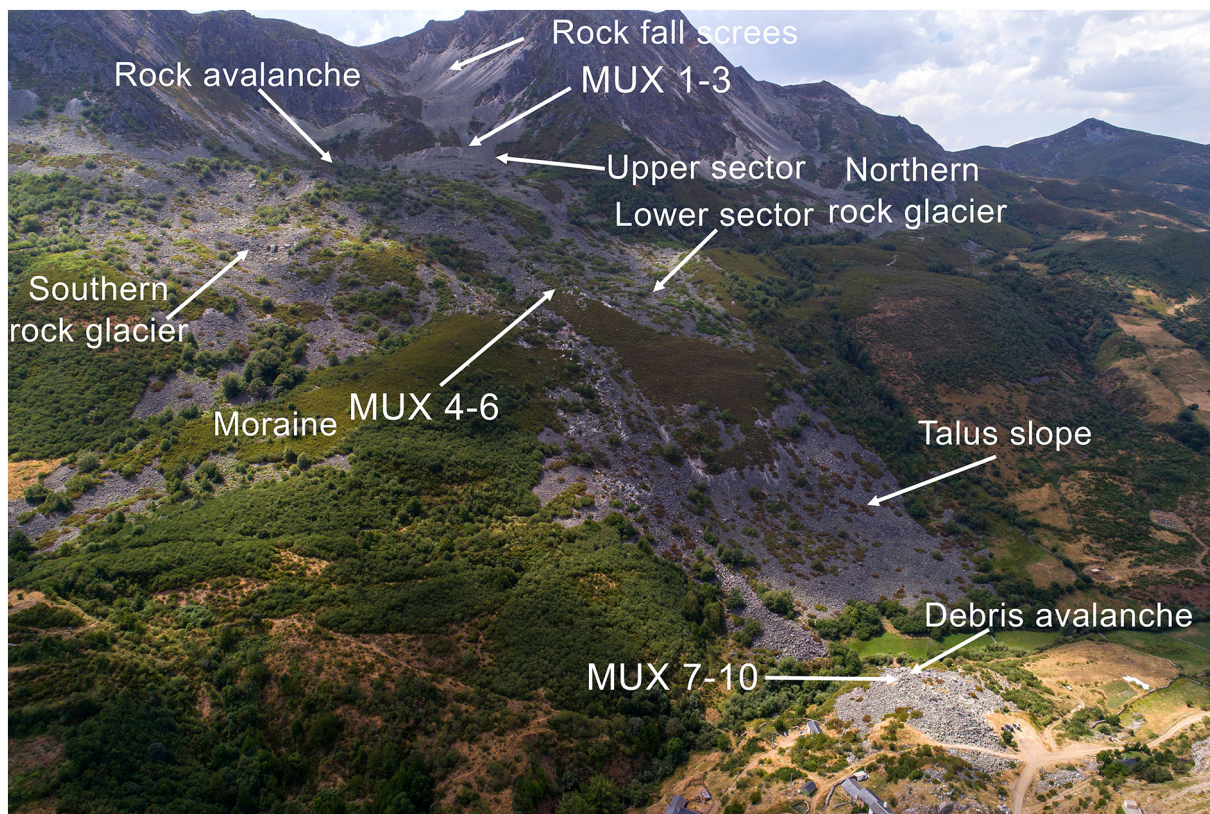


Fig. 3. UAV photograph of the eastern slope of the Muxivén Peak including the main deposits and samples examined in the text.

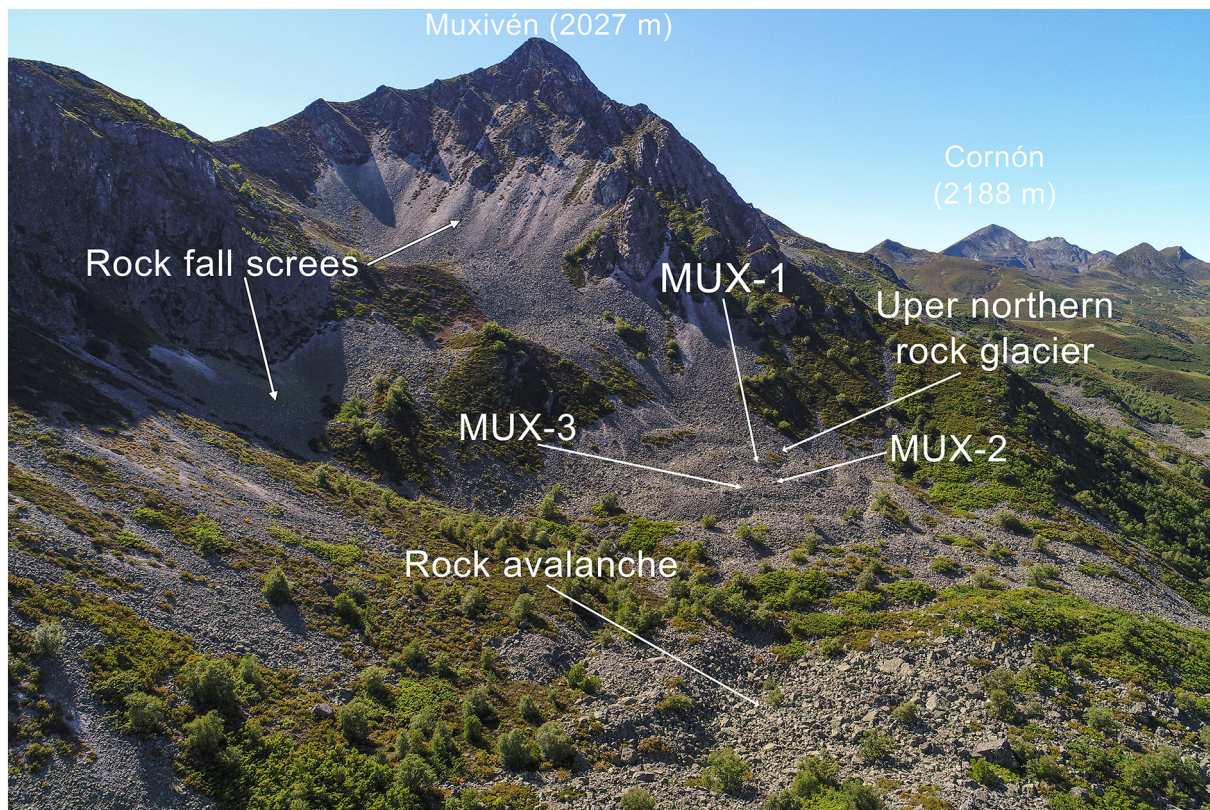
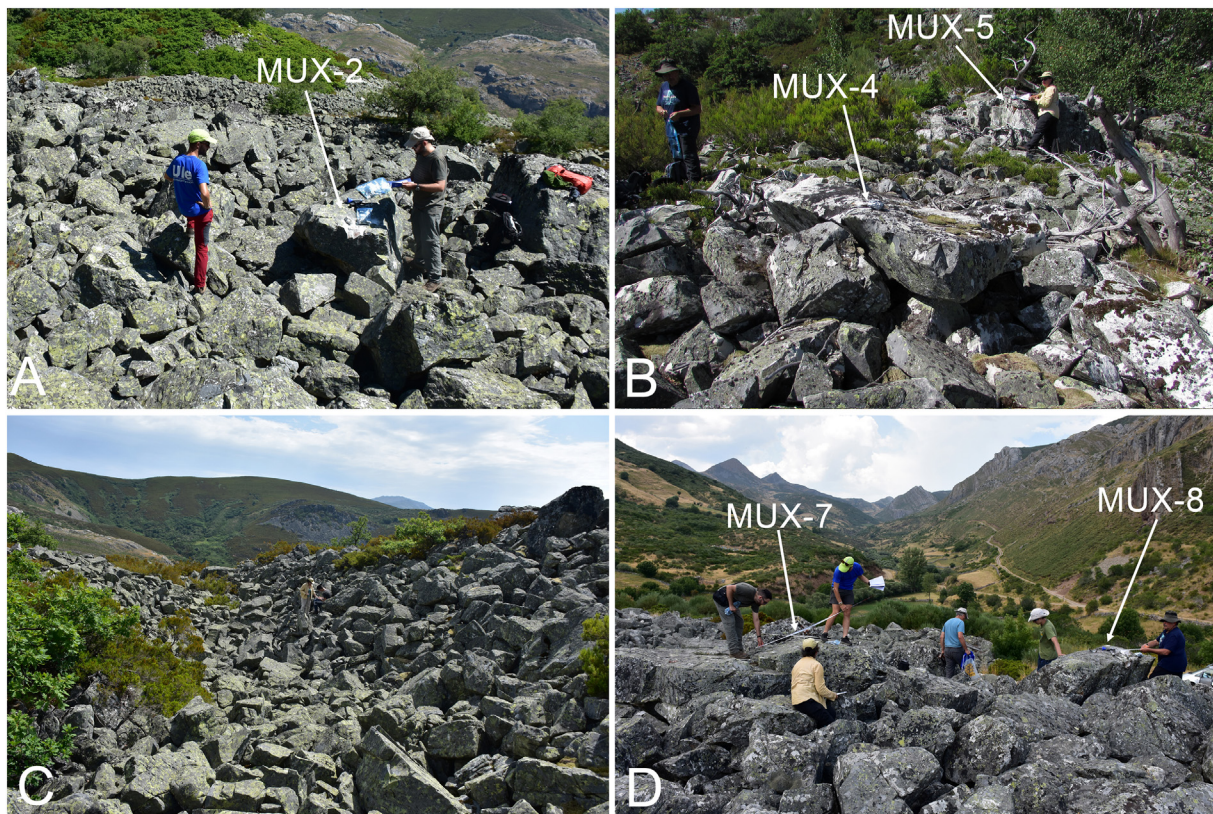


Fig. 4. UAV image from the upper sector of the northern rock glacier showing the well-defined ridge-and-furrow morphology contrasting with the rock avalanche deposit located in the lower part of the image.



**Fig. 5.** (A) Sampling the upper sector of the northern rock glacier. (B) Sampling the lower sector of the northern rock glacier. (C) Series of ridges and furrows existing in the lower sector of the northern rock glacier, where macrofabric analysis were carried out (note the people as for reference scale). (D) Sampling site in the distal part of the debris avalanche deposit.

hammer stations were established in the main units (units ii to vii) to verify possible differences in their SH-R ages (Fig. 2B).

The two sectors of the northern rock glacier were sampled for CRE dating (Fig. 2B). In the upper sector, the sample MUX-1 was collected from an internal ridge, and samples MUX-2 and MUX-3 in the next external one (Fig. 5A). Samples MUX-4, MUX-5 and MUX-6 were collected (Fig. 5B) from the top of a lateral ridge of the lower sector. Finally, given the spatial relationships with the rock glacier, four samples were taken in the frontal deposit of the debris avalanche which come from the margin of the northern rock glacier (MUX-7, MUX-8, MUX-9, MUX-10) (Fig. 5D).

#### 4.2. Sedimentological results

The results of the macrofabric analysis in the sampled sites of the rock glacier and the debris avalanche show similar characteristics. The main vector ( $V_1$ ) slightly matches the slope orientation in all cases (parallel or sub-parallel to the slope in 6 samples and perpendicular to this direction in 3 samples, Fig. 6) and shows a sub-horizontal inclination (dip). In the distal part of the debris avalanche the  $V_1$  dips  $16^\circ$  towards the Muxivén Cirque despite it is located on the opposite slope, in the Lumajo Valley.

The values of  $S_1$ , — degree of concentration around the main direction of the deposit — are very low (around 0.5, Table 2), except in the unit vii (rock fall screens,  $S_1$ : 0.70) and one depression in the upper rock glacier ( $S_1$ : 0.72). This low concentration of  $V_1$  is observed in the fabric shape (Fig. 6), where the stereograms display concentration contours  $<5\%$ , except in the talus slope at the front of the lower sector of the rock glacier, where they reach 12%. So, the majority of the samples show girdle shapes, the talus slopes being the exception, displaying a cluster shape.

The mean block size exceeds 45 cm major axis in all units (Fig. 7). The highest mean block size occurs in the southern rock glacier, in the debris avalanche deposits and the lower sector of the lower rock glacier (Fig. 7).

#### 4.3. Schmidt-hammer dating

SH-R results show similar mean R-values across the 102 studied boulders, ranging from 73 to 79.9 (Fig. 8; Table 3). At each site, mean differences of 5.8 points (between 2.1 and 10.4) occurred between the maximum and minimum R- values of the six sampled boulders, while these differences accounted for 8.3 points at each single boulder.

The highest mean R- value found was 79.9 (Fig. 8), in the rock fall screens. Five boulders of this deposit show values over 79.5 and are in the nine higher values. The second higher value was obtained in the internal ridge of the lower section of the rock glacier, with R of 77.2. The results in the rest of the units show very similar mean R- values ranging from 76.8 to 75.0 (Table 3), except for the rock avalanche deposits (74.2) and one sample in the debris avalanche (73.0), which display slightly lower values.

#### 4.4. CRE ages chronology

Three sampled boulders (MUX-4, MUX-5 and MUX-6) in the right (southern) margin of the lower sector of the rock glacier yielded exposure ages of  $12.4 \pm 0.9$ ,  $14.9 \pm 1.0$ , and  $14.2 \pm 2.5$  ka. Exposure ages from two adjacent ridges in the upper sector of the rock glacier, yielded slightly younger exposure ages of  $13.3 \pm 0.9$ ,  $13.9 \pm 0.8$  and  $13.4 \pm 0.8$  ka respectively (samples MUX-1, MUX-2 and MUX-3; Table 4, total uncertainty), indicative of the stabilization of the highest —and hence youngest— generation of the rock glacier. The chi-2 test (according to

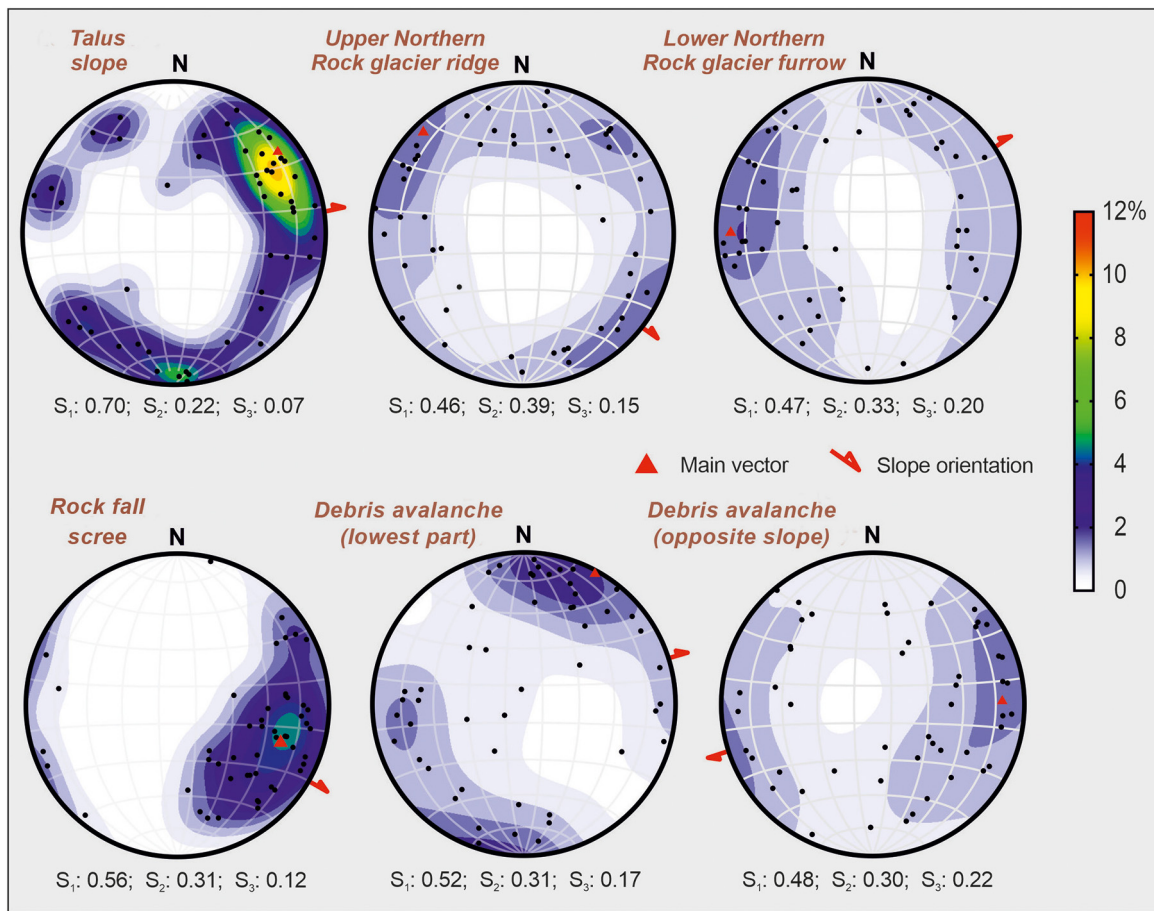


Fig. 6. Representative fabric shape of selected samples distributed across the different landforms.

Ward and Wilson, 1978) showed that the three exposure ages within each geomorphological unit are consistent with each other and thus, no potential outliers were detected.

Finally, the three sampled boulders at the distal part of the debris avalanche yielded exposure ages of  $13.5 \pm 0.8$ ,  $14.0 \pm 1.0$ ,  $14.4 \pm 0.9$  ka and  $19.7 \pm 1.7$  ka (samples MUX-7, MUX-8, MUX-10 and MUX-9; Table 4). The chi-2 test identified the sample MUX-9 as a potential outlier. No spatial pattern has been detected from the CRE ages at this site.

## 5. Analysis of results and discussion

### 5.1. Geomorphological evolution of the eastern slope of the Muxivén Cirque

#### 5.1.1. Geomorphological interpretation

Our results allow us to proposed a reconstruction the geomorphological sequence occurred in the Muxivén Cirque during the final deglaciation of the Lumajo Valley:

- (i) Small glaciers occupied the bottom of the cirque at the end of deglaciation, as evidenced by the moraine that closes the base of the cirque. The alignment of the moraine and its lithological composition indicate that the glacier flowed from the cirque, and not from the main Lumajo valley. In addition, the absence of large boulders and a clear single ridge indicates that it corresponded to a debris-free glacier.
- (ii) Subsequently, as glaciers retreated, large rock avalanches occurred on the cirque wall, whose scar is still well-preserved. In fact, many valleys and cirque floors of the River Sil basin are affected by different types of landslides and avalanches, indicating intense paraglacial dynamics (Santos-González et al., 2018), as it

usually occurs in many deglaciated valleys (Ballantyne, 2002; Linge et al., 2020). The rock avalanche deposits, including many boulders exceeding 4 m of longest axis, covered the upper part of the aforementioned moraine. The rock avalanche deposits show a spatial connection with the margins of the rock glaciers.

- (iii) We assume that these rock avalanches contributed to the formation of the rock glaciers. The precedence of the rock glacier debris is supported by the sedimentological analysis: the debris sizes at the lower sector of the northern rock glacier and the southern rock glacier are very similar to the rock avalanche deposits, both including boulders over 4 m of long axis (Fig. 7), unlike the talus slopes that covered the cirque. In addition, the roots of the rock glaciers - except the upper sector of the northern one, as discussed later - are topographically connected with the rock avalanche deposits. The large size of the boulders is a common characteristic of the “paraglacial rock glaciers”, where debris was supplied by rock avalanches and the subsurface ice originated from a retreating glacier; therefore, they are interpreted as “glacier-derived rock glaciers” (Knight et al., 2019). This process has been identified in many mountain areas where paraglacial processes were dominant (Johnson, 1984; Berthling, 2011; Janke et al., 2015; Hartvich et al., 2017; Monnier and Kinnard, 2017; Anderson et al., 2018; Knight et al., 2019; Etzelmüller et al., 2020; Fernández-Fernández et al., 2020; Linge et al., 2020; Charton et al., 2021; Palacios et al., 2021; RGIK, 2021; Tanarro et al., 2021).

The lower altitudinal limits of the Muxivén rock glaciers are similar to other rock glaciers existing in this range (Gómez-Villar et al., 2011), which could be indicative of the lower limit of discontinuous permafrost in the past (Kerschner, 1978; Giraudi

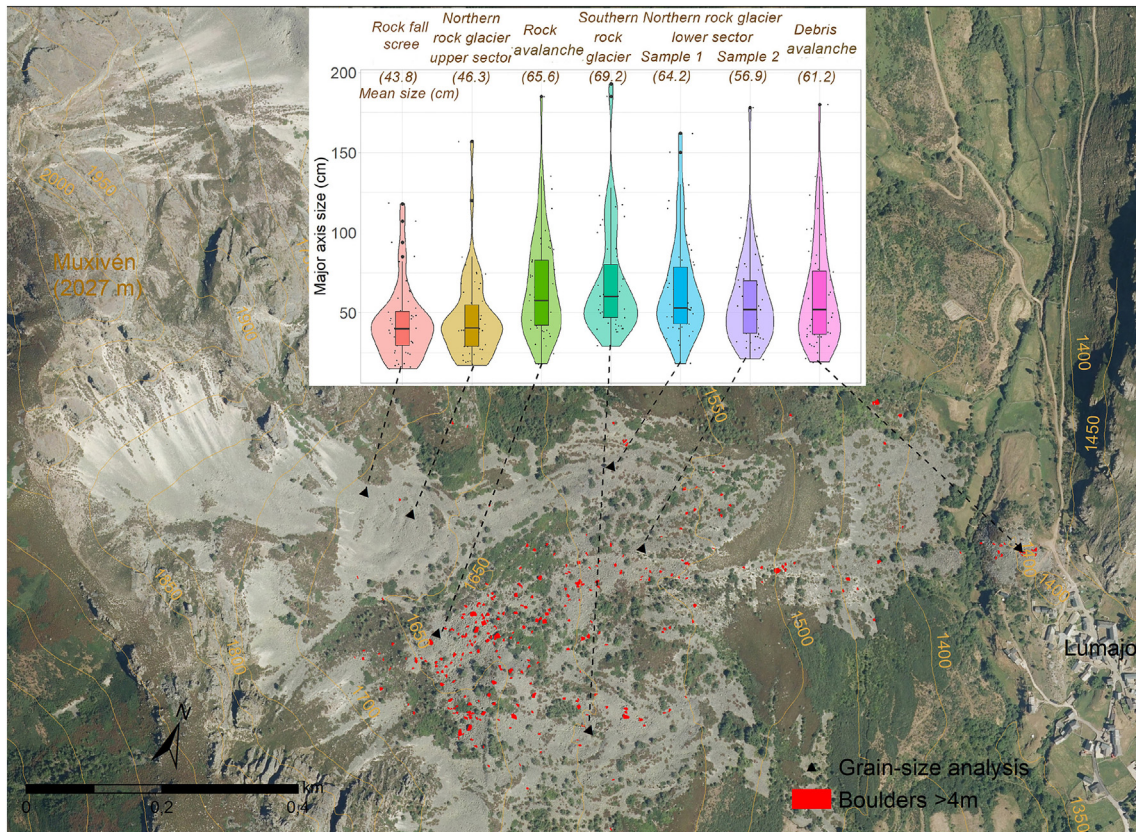


Fig. 7. Distribution of the large boulders >4 m of major axis size together with the grain size data (mean size of the main axis in brackets) of the main deposits in the study area.

and Frezzotti, 1997; Hughes et al., 2003). Nevertheless, rock glacier distribution in the Cantabrian Mountains (Gómez-Villar et al., 2011) is restricted to glacial cirques (Santos-González et al., 2018), which show a limited altitudinal range (Gómez-Villar et al., 2015). In the case of Muxivén rock glaciers, its location is conditioned by the presence of steep glacial escarpments that facilitate rock avalanches.

(iv) Rock glaciers expanded, particularly the northern one, while the southern developed a less defined morphology, probably due to a less lasting activity. The northern rock glacier, with its

headwaters at a higher altitude and a larger and more favourable feeding area, evolved towards a more mature rock glacier morphology and subdivided in two sectors; the upper one was fed only by rock fall scree (including smaller clast size; Fig. 7) and overlapped the lower one, as previously noticed by Rodríguez et al. (2020). This sector also shows a clearer transversal ridge and furrow morphology with fewer collapses. So this sector is considered a talus-derived rock glacier.

(v) At the southern margin of the northern rock glacier, a high-energy debris avalanche occurred, which descended to the valley

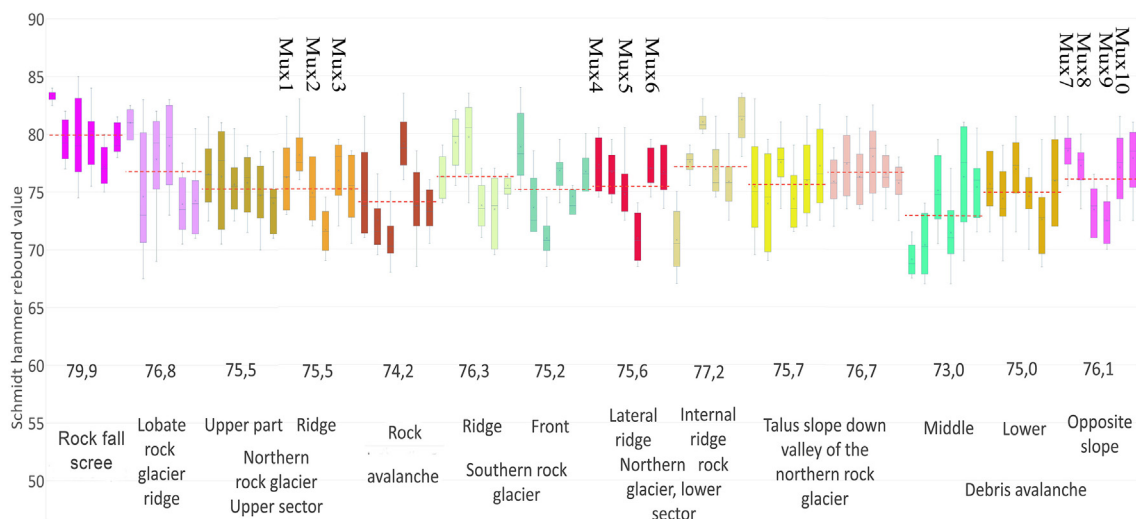


Fig. 8. Schmidt-hammer rebound (R-) values in the different landforms, including the distribution of the samples obtained for CRE dating.

**Table 3**  
Schmidt-hammer rebound values data in each landform.

Samples		Number of boulders sampled	Mean	Standard deviation	Boulder maximum mean	Boulder minimum mean
Rock fall scree		6	79.9	2.78	83.4	77.2
Relict creep talus		6	76.8	4.41	81.0	74.0
Upper northern rock glacier	Upper part	6	75.5	2.96	76.6	74.1
	Ridge	6	75.5	3.21	78.2	71.7
Rock avalanche		6	74.2	3.86	79.2	71.5
Southern rock glacier	Ridge	6	76.3	3.32	79.7	73.5
Lower northern rock glacier	Internal ridge	6	75.2	3.34	78.9	71.0
	Lateral ridge	6	75.6	3.13	77.3	71.0
	Frontal ridge	6	77.2	4.00	81.2	70.8
Talus slope		6	75.7	3.50	77.5	74.0
Debris avalanche	Middle	6	73.0	4.02	76.3	69.2
	Lower	6	75.0	3.14	77.0	72.6
	Opposite slope	6	76.1	3.19	78.6	72.5

floor and even climbed several tens of metres up the slope. Due to its sedimentological characteristics, an unsaturated flow is inferred. It is composed of large boulders released from the rock avalanche, thus indicating a younger age.

- (vi) Subsequently, the cirque probably underwent a phase of geomorphic stability, except for rock falls on the highest talus slopes from the headwall, with creep talus in favourable areas. The rock falls still persist today in the highest areas.

The sedimentological analysis showed that the sampled deposits are associated with the deglaciation of this cirque (and not with the main Lumajo Valley). Macrofabric analysis do not show a clear difference on the origin of each of the deposits, as they near all of them come from massive flows, although with different types of transport (rock glaciers, massive rock movements). Due to that, fabrics are girdle and  $S_1$  values are low, as usually occur in relict rock glaciers and landslides (González-Gutiérrez et al., 2019). The talus slopes derived either from rock falls from the rock glacier front or the wall are the only features showing a cluster fabric.

5.1.2. Chronological reconstruction based on  $^{10}\text{Be}$  CRE and SH-R

CRE results are limited to the two sectors of the northern rock glacier and the debris avalanche. Only the results of one sample that yielded  $19.7 \pm 1.7$  ka (MUX-9) do not follow the logical chronostratigraphical sequence, as it is much older than samples located around and above it. In addition to this, the chi-2 test gives ground to consider this sample

as an outlier. The interpretation of this exposure age is not straight forward, and we hypothesize on two plausible scenarios as it could be either (i) a moraine boulder fallen from the upper part of the slope, thus leading to an anomalously old exposure age; or (ii) a boulder directly fallen from the cirque wall, inefficiently eroded during its displacement, and thus retaining an inherited  $^{10}\text{Be}$  inventory whose corresponding apparent exposure age does not indicate to the deposition of the boulder (Çiner et al., 2017). The latter hypothesis seems less plausible, since the SH-R data also show clearly lower value than the other samples. The rest of the three boulders at the debris avalanche front gave very similar exposure ages, with an arithmetic mean of  $14.0 \pm 0.9$  ka. Two of the three boulders sampled in the lower sector of the northern rock glacier gave very similar ages, averaging  $14.5 \pm 1.5$  ka, while the third one is younger,  $12.4 \pm 0.9$  ka, and may indicate a subsequent remobilization driven by the degradation of this landform. The three blocks sampled in the upper sector of the northern rock glacier gave identical ages, with an average of  $13.5 \pm 0.8$  ka, which may indicate a later stabilization at higher elevations.

Plotting  $^{10}\text{Be}$  exposure ages against SH-R values (Fig. 9A) yielded a coefficient of determination  $R^2 = 0.65$ , i.e. a moderate correlation. Correlations and line tendency using maximum SH-R value instead of the mean value show very similar results ( $R^2$  0.60). Nine of the boulders showed quite similar medium SH-R values (74.8 to 78.6). The only external value is obtained in the outlier MUX-9 that show SH-R value of 72.5, coinciding with the different value in  $^{10}\text{Be}$  data (19.7 ka) (Fig. 9A). If this sample is not considered (Fig. 9B), the trendline is

**Table 4**

AMS analytical data and  $^{10}\text{Be}$  exposure ages.  $^{10}\text{Be}/^9\text{Be}$  ratios were inferred from measurements at the ASTER AMS facility. The numbers in italics correspond to the internal (analytical) uncertainty at 1 $\sigma$  level.

$^{10}\text{Be}$ samples analytical AMS data						
Sample name	Quartz weight (g)	Mass of carrier ( $^9\text{Be}$ mg)	$^{10}\text{Be}/^9\text{Be}$ ( $10^{-14}$ )	Blank correction (%)	$[^{10}\text{Be}]$ ( $10^4$ atoms $\text{g}^{-1}$ )	$^{10}\text{Be}$ exposure ages (ka)
Upper northern rock glacier						
MUX-1	14.8012	0.4831	$8.508 \pm 0.395$	1.28	$18.310 \pm 0.866$	$13.3 \pm 0.9$ (0.6)
MUX-2	19.1102	0.4801	$11.426 \pm 0.400$	0.96	$18.991 \pm 0.675$	$13.9 \pm 0.8$ (0.5)
MUX-3	17.4239	0.4746	$10.091 \pm 0.391$	1.10	$18.162 \pm 0.715$	$13.4 \pm 0.8$ (0.5)
Lower northern rock glacier						
MUX-4	15.8336	0.4752	$8.369 \pm 0.511$	2.28	$16.401 \pm 1.034$	$12.4 \pm 0.9$ (0.8)
MUX-5	8.4065	0.4783	$5.418 \pm 0.305$	3.49	$19.870 \pm 1.184$	$14.9 \pm 1.0$ (0.8)
MUX-6	15.7994	0.4822	$9.595 \pm 1.715$	1.96	$19.178 \pm 3.501$	$14.2 \pm 2.5$ (2.4)
Debris avalanche						
MUX-7	18.8113	0.4804	$9.563 \pm 0.334$	1.97	$15.992 \pm 0.582$	$13.5 \pm 0.8$ (0.5)
MUX-8	13.0661	0.4731	$6.962 \pm 0.386$	2.75	$16.383 \pm 0.948$	$14.0 \pm 1.0$ (0.8)
MUX-9	19.5324	0.4677	$14.321 \pm 1.172$	0.79	$22.731 \pm 1.877$	$19.7 \pm 1.7$ (1.5)
MUX-10	15.3757	0.4547	$8.469 \pm 0.391$	1.37	$16.511 \pm 0.776$	$14.4 \pm 0.9$ (0.6)
Chemistry blank data						
Blank name	Processed with	Mass of carrier ( $^9\text{Be}$ mg)	$^{10}\text{Be}/^9\text{Be}$ ( $10^{-14}$ )		$[^{10}\text{Be}]$ ( $10^4$ atoms)	
BK-15	MUX-4, 5, 6, 7, 8	0.4731			$0.191 \pm 0.063$	$6.051 \pm 1.984$
BK-16	MUX-1, 2, 3, 9, 10	0.4665			$0.113 \pm 0.029$	$3.526 \pm 0.903$

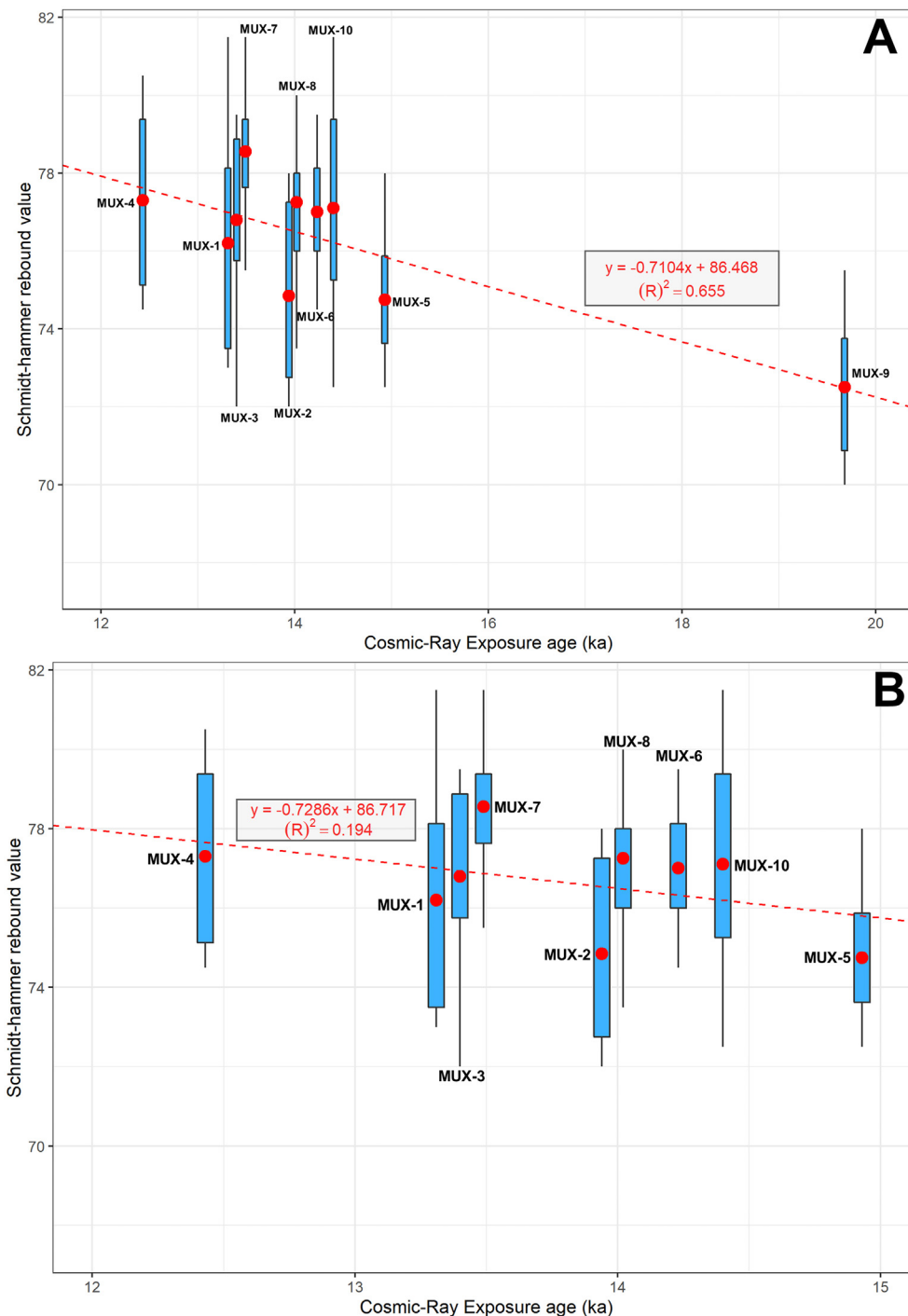


Fig. 9. Correlation between mean SH-R values and <sup>10</sup>Be CRE ages. A: all samples included. B: all samples except MUX-9 included.

very similar but correlation is very low ( $R^2 = 0.19$ ). Anyway, age differences are also very negligible. Probably because these low age differences in Muxivén samples, correlations between SH-R and CRE are lower than previous works (e.g. Tomkins et al., 2016). In any case, the degree of uncertainty of the SH-R results only allows us to determine that debris avalanche and rock glacier boulders show very similar SH-R values, so it is reasonable to hypothesize on both having a similar age. The SH-R values also indicate that the rock avalanche deposits is slightly older or very similar in age, and that boulders from the rock fall scree are clearly younger than the rest of the analysed deposits. In addition, the similarity of CRE ages in each sampled site of the northern rock glacier and the debris avalanche (Fig. 10) does allow us to establish

a chronology in good agreement with the previously determined geomorphological phases:

- (i) Although the moraine could not be dated due to the absence of suitable boulders, it must have been formed during the deglaciation of the main valley, when the glacier was restricted to the cirque, likely at 16 cal ka BP (Jalut et al., 2010).
- (ii) The probably polygenic rock avalanches must have occurred slightly before and during the formation of rock glaciers, as proposed by the SH-R results and the geomorphological reconstructions, in any case between 16 and 14.5 ka.
- (iii) The rock glacier expanded, but the lower sector of the northern

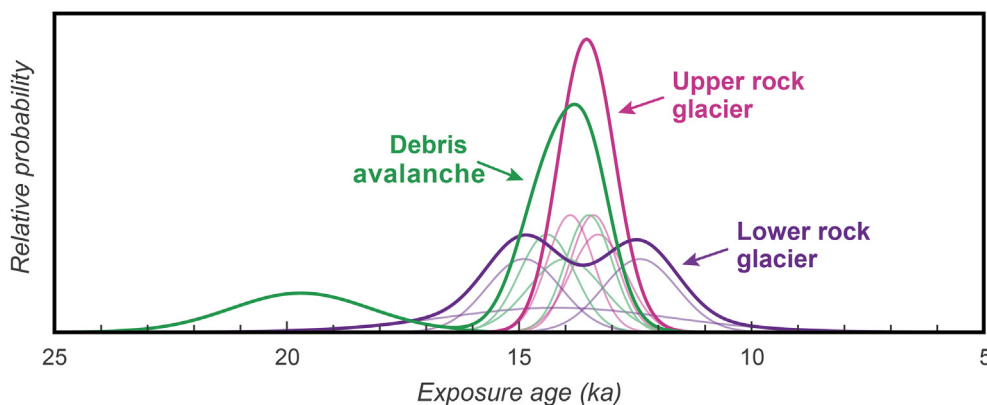


Fig. 10. Probability density plots of CRE ages for differentiated geomorphological units: upper and lower sectors of the northern rock glacier and debris avalanche.

rock glacier definitively stabilized at  $14.5 \pm 1.5$  ka. However, the upper sector remained active slightly longer given its higher elevation and the more dynamic feeding area (rock fall screens), stabilising at  $13.5 \pm 0.8$  ka.

- (iv) The younger debris avalanche occurred concurrently with the stabilization of the lower northern rock glacier front at  $14.0 \pm 0.9$  ka.
- (v) The rock fall screens show limited activity at present, being more dynamic in the highest areas.

Although nuclide inheritance may be common in some rock glaciers (Çiner et al., 2017), the fact that the boulder exposure ages of the Muxivén rock glaciers are either fully coincident or somewhat younger than those closer to the headwall, may rule out this scenario. In fact, nuclide inheritance has been also discarded in the dating of boulders of many other small rock glaciers in Iberia (Palacios et al., 2016, 2017, 2020; Rodríguez-Rodríguez et al., 2017; Andrés et al., 2018; García-Ruiz et al., 2020; Oliva et al., 2021). However, the sample MUX-9, collected from the debris avalanche, is considered to retain nuclide inheritance, not removed during the avalanche event, which is very common in this type of mass movements (Hughes et al., 2014).

### 5.2. The Bølling-Allerød interstadial in the Iberian Peninsula and its role on the rock glacier development

The results obtained from the Muxivén rock glaciers show ages ( $14.0 \pm 0.9$  ka and  $13.5 \pm 0.8$  ka) close to that of the two other rock glaciers dated so far in the Cantabrian Mountains: at Porma River (Requejines cirque), at the southern slope of the mountains ( $15.7 \pm 0.8$  ka; Rodríguez-Rodríguez et al., 2016) and in the headwaters of the Monasterio River at the northern slope of the mountains ( $13.0 \pm 0.5$  ka), the latter being located upslope a moraine with an age of  $14.0 \pm 0.6$  ka (Rodríguez-Rodríguez et al., 2017). Similar geomorphological sequences, with small moraines and rock glaciers in the cirques are common in many sectors of the Cantabrian Mountains, although their minimum ages are only poorly defined through radiocarbon dating applied to lacustrine sediments or peat bogs, but they do confirm that they formed around 15 ka (Pellitero, 2021; Santos-González et al., 2021). Similar landforms have been found in the Central (Cateras, Piniécho and Brazato cirques in the Gállego catchment; Palacios et al., 2017) and Eastern (Malniu and Perafita cirques; Andrés et al., 2018) Pyrenees, also with ages ranging from 16 ka for the moraines to 15–14 ka for the rock glacier fronts. In the Iberian Range, to the south-east of the study area, a date from a rock glacier in Peña Negra (Sierra Cebollera) reported its definitive stabilization at 15–14 ka, following the glacier withdrawal from the moraine at 16 ka (García-Ruiz et al., 2020).

Such a relatively frequent chronological sequence in the cirques is well known in the Iberian mountains and is summarized in four main stages: (i) moraines deposited in a previous glacial advance at ~16 ka

(GS-2.1a, following Rasmussen et al., 2014); (ii) a rapid glacial retreat at ~15 ka (GS-2.1a); (iii) the formation of rock glaciers when paraglacial processes, as rock avalanches, cover the retreating glaciers; and (iv) a rapid stabilization of the rock glacier fronts at 15–14 ka (GI-1e, GI-1d). This sequence is fully coherent with the well-studied climatic evolution in the Iberian Peninsula, which underwent one of the most abrupt climatic changes of the Late Pleistocene at the end of the very cold Heinrich Stadial-1 (HS-1) (Cacho, 2021). Its effects on the Iberian climate ended at 15.7–15.2 cal ka BP, according to different terrestrial (Camuera et al., 2021) and marine (Martrat et al., 2014; Ausín et al., 2020) proxies. Around 15 cal ka BP, the sea surface temperature increased  $4^\circ\text{C}$  on average around the Iberian Peninsula (Cacho et al., 2001; Rodrigo-Gámiz et al., 2014) and warm air temperatures similar to the present-day values, prevailed during most of the B-A interstadial (Fletcher et al., 2010b). Precipitation increased to near current levels, as reflected in the speleothems (Moreno et al., 2010). The vegetation changed drastically towards a temperate Mediterranean forest throughout the peninsula (Fletcher and Sánchez-Gofi, 2008; Fletcher et al., 2010b; García-Alix et al., 2014; Martrat et al., 2014; Naughton et al., 2016; González-Sampériz et al., 2017; Ausín et al., 2020; López-Sáez et al., 2020; Camuera et al., 2021). The effects of the major changes occurring in the North Atlantic were amplified in the Iberian Peninsula at that time (Cacho, 2021), from the strengthening of the Atlantic Meridional Overturning Circulation (McManus et al., 2004), the sharp decline in the sea ice extent (Denton et al., 2005) and the general warming in the Northern Hemisphere reflected in the Greenland ice-core records (Clark et al., 2012; Rasmussen et al., 2014).

The recent geomorphological information available from the Iberian Peninsula allows us to know the immediate reaction of the glaciers to past warm phases such as the B-A, in the form of a rapid retreat and even their total disappearance (Oliva et al., 2019). In the Cantabrian Mountains (Jiménez-Sánchez et al., 2021; Ruiz-Fernández et al., 2021a,b; Serrano et al., 2021a,b) and Northwestern Mountains of Iberia (Rodríguez-Rodríguez et al., 2021; Pérez-Alberti and Valcárcel, 2021), the valleys were deglaciated by 15–14.5 ka. In the Central Pyrenees, for example, a recent study at Bacivè cirque evidences a rapid deglaciation underway at 15–14 ka (Oliva et al., 2021). In the Iberian Range, most glaciers must have disappeared around 14 ka, except some debris-covered glaciers (García-Ruiz, 2021). In the Central Range, the glaciers retreated from 15.5 ka, and by 14.6 ka they were already confined to the cirques or even had disappeared (Carrasco et al., 2021a, 2021b). In the Sierra Nevada, glaciers started to retreat at an average date of  $14.6 \pm 1.5$  ka, but most of the glaciers of the range had already melted away by 14 ka (Palacios et al., 2016, 2020).

The warm and humid B-A interstadial was interrupted in the Iberian Peninsula by two short cold and dry periods at 14.0 and 13.3 ka, in phase with the cold events detected in the Greenland ice-cores, i.e. the GI-1d (Older Dryas) and GI-1b (Intra-Allerød Cold Period)

(Fletcher et al., 2010a; Bernal-Wormull et al., 2021). Due to the range of uncertainty in the dating methods, it is very difficult to determine the impact of these cold events on the Iberian glaciers and rock glaciers, although in some cases the existence of intra- B-A moraines has been pointed out (Oliva et al., 2021).

The rapid deglaciation of the Iberian mountain cirques triggered the acceleration of paraglacial processes on their walls (Oliva et al., 2019). The origin of many of the Iberian rock glaciers that formed just before or during B-A has been related to the effects of these paraglacial processes on the retreating glaciers (Palacios et al., 2016, 2017, 2020; Andrés et al., 2018; García-Ruiz et al., 2020; Oliva et al., 2021). Thus, this generation of rock glaciers may therefore be related to the coupling between the climate warming, retreat of the glaciers and onset of the paraglacial processes, whose deposits eventually cover and insulate the glaciers, protecting the ice from melting.

The collapse of the rock glaciers at Muxivén represented the definitive disappearance of ice in the cirque. Although small glaciers did exceptionally form on some Iberian mountains during the YD, those only developed at the foot of the highest peaks of the major mountain ranges, but not in mid-altitude mountains such as in the Muxivén area (García-Ruiz et al., 2016).

### 5.3. The palaeoclimatic significance of rock glaciers and the paraglacial influence

The rock glaciers of the Muxivén Cirque may constitute examples for a model explaining the generation of Iberian rock glaciers closely related to the effects of the B-A warming. Their origin is related to shrinking glaciers which triggered paraglacial processes as their surrounding walls remained ice-free, subsequently increasing their self-weight shear stress (Ballantyne, 2002), which supplied great volumes of debris that favoured the partial insulation of the ice from the air temperature fluctuations and the solar radiation (Humlum, 2000), and hence, the rock glacier development. In fact, the Muxivén rock glaciers originated from paraglacial rock avalanches. Different types of large paraglacial avalanches and landslides are relatively frequent in the area (Santos-González et al., 2018). The generation of rock glaciers by secondary creep from rock avalanches in permafrost environments has been previously addressed (Knight et al., 2019; Etzelmüller et al., 2020; RGIK, 2021), suggesting the possible polygenetic nature of some boulder-dominated depositional landforms (Wilson et al., 2020). The transformation of retreating glaciers into rock glaciers due to the paraglacial processes may occur within only a few hundred years, when paraglacial debris supply buried the residual ice during and soon after deglaciation (Linge et al., 2020). This process is what our data seem to indicate happened in Muxivén, as well as in many Iberian rock glaciers.

The insulating potential of ice by the debris layer of the rock glaciers is limited in a climatic context of strong warming. Probably for this reason, the Muxivén rock glaciers stabilized shortly after it developed, as it has also been observed in other cases of the same generation of Iberian rock glaciers (Palacios et al., 2016, 2017, 2020; Rodríguez-Rodríguez et al., 2017; Andrés et al., 2018; García-Ruiz et al., 2020; Oliva et al., 2021) and in many other areas (Humlum, 2000; Hippolyte et al., 2009; Janke et al., 2015; Monnier and Kinnard, 2015; Moran et al., 2016; Dede et al., 2017; Winkler and Lambiel, 2018; Linge et al., 2020). Therefore, the rock glacier remains active and flows long enough to acquire its characteristic morphology of furrows and ridges, transverse to the flow and to form a steep front (Berthling, 2011; Janke et al., 2013, 2015). Muxivén rock glacier history confirms how some rock glaciers can form and deactivate rapidly as a result of a warming climate change, not from a cooling one (Knight et al., 2019; Linge et al., 2020). In this sense, the dichotomy between glacier derived rock glaciers versus talus derived rock glaciers is incomplete (Linge et al., 2020), as it does not include many of the (paraglacial) rock glaciers,

whose ice comes from a glacier and its debris from rock avalanches, reactivated precisely when the upper part of the headwalls are freed from the receding glacier (Knight et al., 2019).

Our exposure age results from the termini of the two rock glaciers generation at Muxivén lead us to hypothesize that the melting of the rock glacier margins, especially when it is on a steep slope, may be responsible of its collapse. Thus, just as the lower sector of the rock glacier was stabilising, a large debris avalanche occurred. This fact could explain why the age of stabilization of the lower sector of the rock glacier ( $14.5 \pm 1.5$  ka) and that of the debris avalanche at its front ( $14.0 \pm 0.9$  ka) is very close. The influence of a warming climate in rock glaciers destabilization has been observed recently in the Alps (Marcer et al., 2021).

The concept of stabilization in a rock glacier is not straightforward. It may relate either to the complete melting of the interstitial ice or, to a stagnant state even when ice is still present. However, CRE dating does not allow differentiating between the such situations when applied to relict formations (Mackay and Marchant, 2016; Crump et al., 2017; Fernández-Fernández et al., 2020; Scherler and Egholm, 2020; Amschwand et al., 2021; Charton et al., 2021). In Muxivén area, the upper sector of the rock glacier stabilized about a thousand years ( $13.5 \pm 0.8$  ka) after the lower sector also did, probably due to a more continue rock fall debris supply from the cirque headwalls, although more samples would be needed to confirm this age difference. In other cases, in the Iberian Peninsula, the Alps and Northern Iceland, it has also been detected that the stabilization process is delayed in the higher altitude sectors of rock glaciers (Palacios et al., 2016, 2017; Andrés et al., 2018; Fernández-Fernández et al., 2020; Steinemann et al., 2020), even until the Mid Holocene (e.g. Palacios et al., 2017).

## 6. Conclusions

The results obtained for the Muxivén Cirque confirm the major role that the warming recorded during the B-A, which caused the glaciers to retreat on the mountains of the Iberian Peninsula, although the melting of the ice was slowed down by the action of paraglacial processes. These processes were the main causes driving the evolution of some glaciers into rock glaciers. In this work, this was confirmed by a dataset of 9 CRE ages that are in good agreement with high-detailed geomorphological reconstruction, sedimentological analysis and SH-R measurements. The rapid collapse of the rock glaciers is demonstrated by the homogeneity of the exposure ages within the B-A.

The main valley where the Muxivén Cirque is located was most likely deglaciated at 16 ka. Subsequently a small glacier remained inside the cirque and left a moraine, of unknown age. Following the glacier withdrawal from this moraine, important rock avalanches occurred in the cirque, favouring the generation of two rock glaciers. The lower frontal sector of the northern one was stabilized at  $14.5 \pm 1.5$  ka, while at higher altitude the upper sector stabilized at  $13.5 \pm 0.8$  ka. A debris avalanche transferred loose clast supported material towards the valley bottom, crossing the stream and remounting to the opposite hillslope at  $14.0 \pm 0.9$  ka, although we cannot confirm whether the movement of the rock glacier could have contributed to trigger the debris avalanche.

Our findings show the Muxivén Cirque as an illustrative example of many Iberian rock glaciers, which were formed during the B-A interstadial. The exposure age results show that these formations were largely active during short periods of time and whose period of maximum activity at their front usually did not exceed a thousand years.

Their origin was closely related to the glacier retreat at the end of the HS-1, when they remained confined to the cirques and their gradual shrinking favoured the paraglacial readjustment of the cirques to the newly ice-free conditions. Therefore, this work confirms again that most rock glaciers in Iberia did not depend mainly on optimal permafrost conditions but on the existence of retreating glaciers and the intensity of paraglacial processes operating on the cirque headwalls in coincidence with the glacial retreat.

## Declaration of competing interest

The authors declare that they have no known competing financial interests or personal relationships that could have appeared to influence the work reported in this paper.

## Acknowledgements

This research was supported by the project LE080G19 (Paleo-environmental significance and relationship with the global change of the Cantabrian Mountains rock glaciers: relative age dating and analysis of the internal structure using electrical tomography), founded by the Junta de Castilla y León and PR108/20-20 (Santander Bank-UCM Projects). José M. Fernández-Fernández is supported by a postdoctoral grant within the NUNANTAR project, funded by the Fundação para a Ciência e Tecnologia of Portugal (PTDC/CTA-GFI/32002/2017). Marc Oliva is supported by the Ramón y Cajal Program (RYC-2015-17597) and by the Research Group ANTALP (Antarctic, Arctic, Alpine Environments; 2017-SGR-1102) funded by the Government of Catalonia. Adrián Melón-Nava was supported by the FPU program from the Spanish Ministerio de Universidades (FPU20/01220). We thank the comments and suggestions made by Dr. Stefan Winkler and Dr. Philip D. Hughes, which have considerably improved the quality of an earlier version of the manuscript.

## Appendix A. Supplementary data

Supplementary data to this article can be found online at <https://doi.org/10.1016/j.geomorph.2022.108112>.

## References

- Alonso, V., Suárez Rodríguez, Á., 2004. Evidencias geomorfológicas de la existencia de un pequeño casquete glaciar en la Comarca de Babia Alta (Cordillera Cantábrica). *Rev. Soc. Geol. Esp.* 17, 61–70.
- Alonso, J.L., Marcos, A., Suárez, A., 2009. Paleogeographic inversion resulting from large out of sequence breaching thrusts: the León Fault (Cantabrian zone, NW Iberia). A new picture of the external Variscan thrust belt in the Ibero-Armorican arc. *Geol. Acta* 7, 451–473. <https://doi.org/10.1344/105.000001449>.
- Amschwand, D., Ivy-Ochs, S., Frehner, M., Steinemann, O., Christl, M., Vockenhuber, C., 2021. Deciphering the evolution of the Bleis Marscha rock glacier (Val d'Err, eastern Switzerland) with cosmogenic nuclide exposure dating, aerial image correlation, and finite-element modelling. *Cryosphere* 15, 2057–2081. <https://doi.org/10.5194/tc-15-2057-2021>.
- Anderson, L.S., Anderson, R.S., 2016. Modeling debris-covered glaciers: response to steady debris deposition. *Cryosphere* 10, 1105–1124. <https://doi.org/10.5194/tc-10-1105-2016>.
- Anderson, R.S., Anderson, L.S., Armstrong, W.H., Rossi, M.W., Crump, S.E., 2018. Glaciation of alpine valleys: the glacier – debris-covered glacier – rock glacier continuum. *Geomorphology* 311, 127–142. <https://doi.org/10.1016/j.geomorph.2018.03.015>.
- Andrés, N., Gómez-Ortiz, A., Fernández-Fernández, J.M., Tanarro, L.M., Salvador-Franch, F., Oliva, M., Palacios, D., 2018. Timing of deglaciation and rock glacier origin in the southeastern Pyrenees: a review and new data. *Boreas* 47, 1050–1071. <https://doi.org/10.1111/bor.12324>.
- Andrews, J.T., 1971. Techniques of till fabric analysis. *Br. Geomorphol. Res. Group, Tech. Bull.* 6, pp. 1–43.
- Arnold, M., Merchel, S., Bourlès, D.L., Braucher, R., Benedetti, L., Finkel, R.C., Aumaître, G., Gottsdang, A., Klein, M., 2010. The French accelerator mass spectrometry facility ASTER: improved performance and developments. *Nucl. Instrum. Methods Phys. Res., Sect. B* 268, 1954–1959. <https://doi.org/10.1016/j.nimb.2010.02.107>.
- Ausín, B., Hodell, D.A., Cutmore, A., Eglinton, T.I., 2020. The impact of abrupt deglacial climate variability on productivity and upwelling on the southwestern Iberian margin. *Quat. Sci. Rev.* 230, 106139. <https://doi.org/10.1016/j.quascirev.2019.106139>.
- Azócar, G.F., Brenning, A., 2010. Hydrological and geomorphological significance of rock glaciers in the dry Andes, Chile (27°–33°S). *Permafrost. Periglac. Process.* 21, 42–53. <https://doi.org/10.1002/ppp.669>.
- Balco, G., Stone, J.O., Lifton, N.A., Dunai, T.J., 2008. A complete and easily accessible means of calculating surface exposure ages or erosion rates from <sup>10</sup>Be and <sup>26</sup>Al measurements. *Quat. Geochronol.* 3. <https://doi.org/10.1016/j.quageo.2007.12.001> 174e195.
- Ballantyne, C.K., 2002. Paraglacial geomorphology. *Quat. Sci. Rev.* 21 (18–19), 1935–2017. [https://doi.org/10.1016/S0277-3791\(02\)00005-7](https://doi.org/10.1016/S0277-3791(02)00005-7).
- Ballantyne, C.K., Black, N.M., Finlay, D.P., 1990. Use of the Schmidt test hammer to detect enhanced boulder weathering under late-lying snowpatches. *Earth Surf. Process. Landf.* 15, 471–474. <https://doi.org/10.1002/esp.3290150510>.
- Benn, D.I., 1994. Fabric shape and the interpretation of sedimentary fabric data. *J. Sediment. Res. A Sediment. Petrol. Process* 64, 910–915. <https://doi.org/10.1306/d4267f05-2b26-11d7-8648000102c1865d>.
- Benn, D.I., Evans, D.J.A., 1996. The interpretation and classification of subglacially-deformed materials. *Quat. Sci. Rev.* 15, 23–52. [https://doi.org/10.1016/0277-3791\(95\)00082-8](https://doi.org/10.1016/0277-3791(95)00082-8).
- Benn, D.I., Ringrose, T.J., 2001. Random variation of fabric eigenvalues: implications for the use of A-axis fabric data to differentiate till facies. *Earth Surf. Process. Landf.* 26, 295–306. [https://doi.org/10.1002/1096-9837\(200103\)26:3<295::AID-ESP159>3.0.CO;2-1](https://doi.org/10.1002/1096-9837(200103)26:3<295::AID-ESP159>3.0.CO;2-1).
- Bernal-Wormull, J.L., Moreno, A., Pérez-Mejías, C., Bartolomé, M., Aranburu, A., Arriolabengoa, M., Iriarte, E., Cacho, I., Spötl, C., Edwards, R.L., Cheng, H., 2021. Immediate temperature response in northern Iberia to last deglacial changes in the North Atlantic. *Geology* 49. <https://doi.org/10.1130/G48660.1>.
- Berthling, I., 2011. Beyond confusion: rock glaciers as cryo-conditioned landforms. *Geomorphology* 131, 98–106. <https://doi.org/10.1016/j.geomorph.2011.05.002>.
- Braucher, R., Guillou, V., Bourlès, D.L., Arnold, M., Aumaître, G., Keddadouche, K., Nottoli, E., 2015. Preparation of ASTER in-house 10Be/9Be standard solutions. *Nucl. Instrum. Methods Phys. Res., Sect. B* 361, 335–340. <https://doi.org/10.1016/j.nimb.2015.06.012>.
- Brenning, A., 2005. Geomorphological, hydrological and climatic significance of rock glaciers in the Andes of Central Chile (33–35°S). *Permafrost. Periglac. Process.* 16, 231–240. <https://doi.org/10.1002/ppp.528>.
- Cacho, I., 2021. Quaternary ice ages in the Iberian Peninsula. In: Oliva, M., Palacios, D., Fernández-Fernández, J.M. (Eds.), *Iberia, Land of Glaciers*. Elsevier, pp. 13–35. <https://doi.org/10.1016/B978-0-12-821941-6.00002-5>.
- Cacho, I., Grimalt, J.O., Canals, M., Sbaifi, L., Shackleton, N.J., Schönfeld, J., Zahn, R., 2001. Variability of the western Mediterranean Sea surface temperature during the last 25,000 years and its connection with the Northern Hemisphere climatic changes. *Paleoceanography* 16, 40–52. <https://doi.org/10.1029/2000PA000502>.
- Campos, N., Tanarro, L.M., Palacios, D., Zamorano, J.J., 2019. Slow dynamics in debris-covered and rock glaciers in Hofsdalur, Tröllaskagi Peninsula (northern Iceland). *Geomorphology* 342, 61–77. <https://doi.org/10.1016/j.geomorph.2019.06.005>.
- Camuera, J., Jiménez-Moreno, G., Ramos-Román, M.J., García-Alix, A., Jiménez-Espejo, F.J., Toney, J.L., Anderson, R.S., 2021. Chronological control and centennial-scale climatic subdivisions of the last Glacial termination in the western Mediterranean region. *Quat. Sci. Rev.* 255, 106814. <https://doi.org/10.1016/j.quascirev.2021.106814>.
- Carrasco, R.M., Pedraza, J., Palacios, D., 2021a. The glaciers of the Sierra de Gredos. In: Oliva, M., Palacios, D., Fernández-Fernández, J.M. (Eds.), *Iberia, Land of Glaciers*. Elsevier, pp. 457–483. <https://doi.org/10.1016/B978-0-12-821941-6.00022-0>.
- Carrasco, R.M., Pedraza, J., Palacios, D., 2021b. The glaciers of the Sierras de Guadarrama and Somosierra. In: Oliva, M., Palacios, D., Fernández-Fernández, J.M. (Eds.), *Iberia, Land of Glaciers*. Elsevier, pp. 485–503. <https://doi.org/10.1016/B978-0-12-821941-6.00023-2>.
- Charton, J., Jomelli, V., Schimmelfennig, I., Verfaillie, D., Favier, V., Mokadem, F., Gilbert, A., Brun, F., Aumaître, G., Bourlès, D.L., Keddadouche, K., 2021. A debris-covered glacier at Kerguelen (49°S, 69°E) over the past 15 000 years. *Antarct. Sci.* 33, 103–115. <https://doi.org/10.1017/S0954102020000541>.
- Chmieleff, J., von Blanckenburg, F., Kossert, K., Jakob, D., 2010. Determination of the 10Be half-life by multicollector ICP-MS and liquid scintillation counting. *Nucl. Instrum. Methods Phys. Res., Sect. B* 268, 192–199. <https://doi.org/10.1016/j.nimb.2009.09.012>.
- Çiner, A., Sarıkaya, M.A., Yıldırım, C., 2017. Misleading old age on a young landform? The dilemma of cosmogenic inheritance in surface exposure dating: moraines vs. rock glaciers. *Quat. Geochronol.* 42, 76–88. <https://doi.org/10.1016/j.quageo.2017.07.003>.
- Clark, P.U., Shakun, J.D., Baker, P.A., Bartlein, P.J., Brewer, S., Brook, E., Carlson, A.E., Cheng, H., Kaufman, D.S., Liu, Z., Marchitto, T.M., Mix, A.C., Morrill, C., Otto-Bliesner, B.L., Pahnke, K., Russell, J.M., Whitlock, C., Adkins, J.F., Blois, J.L., Clark, J., Colman, S.M., Curry, W.B., Flower, B.P., He, F., Johnson, T.C., Lynch-Stieglitz, J., Markgraf, V., McManus, J., Mitrovica, J.X., Moreno, P.I., Williams, J.W., 2012. Global climate evolution during the last deglaciation. *Proc. Natl. Acad. Sci.* 109, E1134–E1142. <https://doi.org/10.1073/PNAS.1116619109>.
- Crump, S.E., Anderson, L.S., Miller, G.H., Anderson, R.S., 2017. Interpreting exposure ages from ice-cored moraines: a Neoglacial case study on Baffin Island, Arctic Canada. *J. Quat. Sci.* 32, 1049–1062. <https://doi.org/10.1002/jqs.2979>.
- Dede, V., Çiçek, I., Sarıkaya, M.A., Çiner, A., Uncu, L., 2017. First cosmogenic geochronology from the Lesser Caucasus Late Pleistocene glaciation and rock glacier development in the Karçal Valley, NE Turkey. *Quat. Sci. Rev.* 164, 54–67. <https://doi.org/10.1016/j.quascirev.2017.03.025>.
- Delaloye, R., Lambiel, C., Gärtner-Roer, I., 2010. Overview of rock glacier kinematics research in the Swiss Alps. *Geogr. Helv.* 65, 135–145. <https://doi.org/10.5194/gh-65-135-2010>.
- Deline, P., Akçar, N., Ivy-Ochs, S., Kubik, P.W., 2015. Repeated Holocene rock avalanches onto the Brenva Glacier, Mont Blanc massif, Italy: a chronology. *Quat. Sci. Rev.* 126, 186–200. <https://doi.org/10.1016/j.quascirev.2015.09.004>.
- Denton, G.H., Alley, R.B., Comer, G.C., Broecker, W.S., 2005. The role of seasonality in abrupt climate change. *Quat. Sci. Rev.* 24, 1159–1182. <https://doi.org/10.1016/j.quascirev.2004.12.002>.
- Diggle, P.J., Fisher, N.I., 1985. SPHERE: a contouring program for spherical data. *Comput. Geosci.* 11, 725–766. [https://doi.org/10.1016/0098-3004\(85\)90015-9](https://doi.org/10.1016/0098-3004(85)90015-9).
- Dunne, J., Elmore, D., Muzikar, P., 1999. Scaling factors for the rates of production of cosmogenic nuclides for geometric shielding and attenuation at depth on sloped surfaces. *Geomorphology* 27, 3–11. [https://doi.org/10.1016/S0169-555X\(98\)00086-5](https://doi.org/10.1016/S0169-555X(98)00086-5).
- Emmer, A., Loarte, E.C., Klimeš, J., Vilímek, V., 2015. Recent evolution and degradation of the Bent Jatunraju glacier (Cordillera Blanca, Peru). *Geomorphology* 228, 345–355. <https://doi.org/10.1016/j.geomorph.2014.09.018>.

- Eriksen, H., Rouyet, L., Lauknes, T.R., Berthling, I., Isaksen, K., Hindberg, H., Larsen, Y., Corner, G.D., 2018. Recent acceleration of a Rock Glacier complex, Ådjet, Norway, documented by 62 years of remote sensing observations. *LettGeophys. Res.* 45, 8314–8323. <https://doi.org/10.1029/2018GL077605>.
- Etzelmüller, B., Patton, H., Schomacker, A., Czekirda, J., Girod, L., Hubbard, A., Lilleøren, K.S., Westermann, S., 2020. Icelandic permafrost dynamics since the last Glacial Maximum—model results and geomorphological implications. *Quat. Sci. Rev.* 233, 106236. <https://doi.org/10.1016/j.quascirev.2020.106236>.
- Evans, D.J.A., 2017. *Till: A Glacial Process Sedimentology*, The Cryosp. John Wiley & Sons Ltd, Chichester <https://doi.org/10.1002/9781118652541.fmatter>.
- Evans, D.J., Benn, D.I., 2004. *A Practical Guide to the Study of Glacial Sediments*. Edward Arnold, London.
- Fernández Martínez, E., Fuertes Gutiérrez, I., Alonso Herrero, E., Redondo Vega, J.M., Cortizo Álvarez, J., Gómez Villar, A., Santos-González, J., Herrero Hernández, A., González Gutiérrez, R., 2009. Lugares de Interés Geológico. León. *Fundación Patrimonio Natural, Junta de Castilla y León*.
- Fernández-Fernández, J.M., Palacios, D., García-Ruiz, J.M., Andrés, N., Schimmelpfennig, I., Gómez-Villar, A., Santos-González, J., Álvarez-Martínez, J., Arnáez, J., Úbeda, J., Léanni, L., ASTER Team, 2017. Chronological and geomorphological investigation of fossil debris-covered glaciers in relation to deglaciation processes: a case study in the Sierra de La Demanda, northern Spain. *Quat. Sci. Rev.* 170, 232–249. <https://doi.org/10.1016/j.quascirev.2017.06.034>.
- Fernández-Fernández, J.M., Palacios, D., Andrés, N., Schimmelpfennig, I., Tanarro, L.M., Brynjólfsson, S., López-Acevedo, F.J., Sæmundsson, Þ., Team, A.S.T.E.R., 2020. Constraints on the timing of debris-covered and rock glaciers: an exploratory case study in the Hólar area, northern Iceland. *Geomorphology* 361, 107196. <https://doi.org/10.1016/j.geomorph.2020.107196>.
- Fletcher, W.J., Sánchez-Goñi, M.F., 2008. Orbital- and sub-orbital-scale climate impacts on vegetation of the western Mediterranean basin over the last 48,000 yr. *Quat. Res.* 70, 451–464. <https://doi.org/10.1016/j.yqres.2008.07.002>.
- Fletcher, W.J., Sánchez-Goñi, M.F., Allen, J.R.M., Cheddadi, R., Combourieu-Nebout, N., Huntley, B., Lawson, I., Londeix, L., Magri, D., Margari, V., Müller, U.C., Naughton, F., Novenko, E., Roucoux, K., Tzedakis, P.C., 2010a. Millennial-scale variability during the last glacial in vegetation records from Europe. *Quat. Sci. Rev.* <https://doi.org/10.1016/j.quascirev.2009.11.015>.
- Fletcher, W.J., Sánchez-Goñi, M.F., Peyron, O., Dormoy, I., 2010b. Abrupt climate changes of the last deglaciation detected in a Western Mediterranean forest record. *Clim. Past* 6, 245–264. <https://doi.org/10.5194/CP-6-245-2010>.
- French, H.M., 2017. *The Periglacial Environment*. John Wiley & Sons.
- García de Celis, A., 1997. *El relieve de la Montaña Occidental de León*. Universidad de Valladolid, Valladolid.
- García de Celis, A., Martínez Fernández, L.C., 2002. *Morfología glacial de las montañas de la cuenca alta de los ríos Sil, Omaña, Luna y Bernesga: revisión y nuevos datos (Montaña Occidental de León)*. In: Redondo Vega, J.M., Gómez Villar, A., González Gutiérrez, R.B., Carrera Gómez, P. (Eds.), *El Modelado de Origen Glacial En Las Montañas Leonesas*. Universidad de León, León, pp. 137–196.
- García-Alix, A., Jiménez-Moreno, G., Jiménez-Espejo, F.J., García-García, F., Delgado Huertas, A., 2014. An environmental snapshot of the Bölling interstadial in Southern Iberia. *Quat. Res.* 81, 284–294. <https://doi.org/10.1016/j.yqres.2014.01.009>.
- García-Ruiz, J.M., 2021. The glaciers of the Iberian Range. In: Oliva, M., Palacios, D., Fernández-Fernández, J.M. (Eds.), *Iberia, Land of Glaciers*. Elsevier, pp. 437–455. <https://doi.org/10.1016/B978-0-12-821941-6.00023-2>.
- García-Ruiz, J.M., Palacios, D., González-Sampérez, P., Andrés, N., Moreno, A., Valero-Garcés, B., Gómez-Villar, A., 2016. Mountain glacier evolution in the Iberian Peninsula during the Younger Dryas. *Quat. Sci. Rev.* 138, 16–30. <https://doi.org/10.1016/j.quascirev.2016.02.022>.
- García-Ruiz, J.M., Palacios, D., Fernández-Fernández, J.M., Andrés, N., Arnáez, J., Gómez-Villar, A., Santos-González, J., Álvarez-Martínez, J., Lana-Renault, N., Léanni, L., 2020. Glacial stages in the Peña Negra valley, Iberian Range, northern Iberian Peninsula: assessing the importance of the glacial record in small cirques in a marginal mountain area. *Geomorphology* 362, 107195. <https://doi.org/10.1016/j.geomorph.2020.107195>.
- Giraudi, C., Frezzotti, M., 1997. Late Pleistocene glacial events in the Central Apennines, Italy. *Quat. Res.* 48, 280–290. <https://doi.org/10.1006/qres.1997.1928>.
- Gómez-Ortiz, A., Oliva, M., Salvador-Franch, F., Salvà-Catarineu, M., Palacios, D., Sanjosé, J.J., Tanarro, L., Galindo-Zaldívar, J., Sanz de Galdeano, C., 2014. Degradation of buried ice and permafrost in the Veleta cirque (Sierra Nevada, Spain) from 2006–2013. *Solid Earth* 5, 979–993. <https://doi.org/10.5194/se-5-979-2014>.
- Gómez-Villar, A., González-Gutiérrez, R.B., Redondo-Vega, J.M., Santos-González, J., 2011. Distribution of relict rock glaciers in the cantabrian mountains (León, Spain). *Cuad. Investig. Geogr.* 37, 49–80. <https://doi.org/10.18172/cig.1256>.
- Gómez-Villar, A., Santos-González, J., González-Gutiérrez, R.B., Redondo-Vega, J.M., 2015. Glacial cirques in the southern side of the Cantabrian Mountains of southwestern Europe. *Geogr. Ann.*, Ser. A 97 (4), 633–651. <https://doi.org/10.1111/geoa.12104>.
- González-Gutiérrez, R.B., Santos-González, J., Gómez-Villar, A., Redondo-Vega, J.M., 2019. Surface macro-fabric analysis of relict rock glaciers in the Cantabrian Mountains (NW Spain). *Permafrost. Periglac. Process.* 30, 348–363. <https://doi.org/10.1002/ppp.2025>.
- González-Sampérez, P., Aranbarri, J., Pérez-Sanz, A., Gil-Romera, G., Moreno, A., Leunda, M., Sevilla-Callejo, M., Corella, J.P., Morellón, M., Oliva, B., Valero-Garcés, B., 2017. Environmental and climate change in the southern Central Pyrenees since the last Glacial Maximum: a view from the lake records. *Catena* 149, 668–688. <https://doi.org/10.1016/j.catena.2016.07.041>.
- Gosse, J.C., Phillips, F.M., 2001. Terrestrial in situ cosmogenic nuclides: theory and application. *Quat. Sci. Rev.* 20, 1475–1560. [https://doi.org/10.1016/S0277-3791\(00\)00171-2](https://doi.org/10.1016/S0277-3791(00)00171-2).
- Goudie, A.S., 2006. The Schmidt Hammer in geomorphological research. *Prog. Phys. Geogr.* 30, 1073–1087. <https://doi.org/10.1177/0309133306071954>.
- Guglielmin, M., Worland, M.R., Convey, P., Cannone, N., 2012. Schmidt Hammer studies in the maritime Antarctic: Application to dating Holocene deglaciation and estimating the effects of macrolichens on rock weathering. *Geomorphology* 155, 34–44. <https://doi.org/10.1016/j.geomorph.2011.12.015>.
- Haeblerli, W., 1985. *Creep of mountain permafrost: internal structure and flow of alpine rock glaciers*. Mitteilungen der Versuchsanstalt für Wasserbau, Hydrologie und Glaziologie an der Eidgenössischen Technischen Hochschule Zurich. 77 142p.
- Hartvich, F., Blahut, J., Stemberk, J., 2017. Rock avalanche and rock glacier: a compound landform study from Hornsund, Svalbard. *Geomorphology* 276, 244–256. <https://doi.org/10.1016/j.geomorph.2016.10.008>.
- Hippolyte, J.C., Bourliès, D., Braucher, R., Carcaillet, J., Léanni, L., Arnold, M., Aumaitre, G., 2009. Cosmogenic <sup>10</sup>Be dating of a sacking and its faulted rock glaciers, in the Alps of Savoy (France). *Geomorphology* 108, 312–320. <https://doi.org/10.1016/j.geomorph.2009.02.024>.
- Hughes, P.D., Gibbard, P.L., Woodward, J.C., 2003. Relict rock glaciers as indicators of Mediterranean paleoclimate during the last Glacial Maximum (Late Würmian) in North-west Greece. *J. Quat. Sci.* 18 (5), 431–440. <https://doi.org/10.1002/jqs.764>.
- Hughes, P.D., Fink, D., Fletcher, W.J., Hannah, G., 2014. Catastrophic rock avalanches in a glaciated valley of the High Atlas, Morocco: 10Be exposure ages reveal a 4.5 ka seismic event. *GSA Bull.* 126 (7–8), 1093–1104. <https://doi.org/10.1130/B30894.1>.
- Humlum, O., 2000. The geomorphic significance of rock glaciers: estimates of rock glacier debris volumes and headwall recession rates in West Greenland. *Geomorphology* 35, 41–67. [https://doi.org/10.1016/S0169-555X\(00\)00022-2](https://doi.org/10.1016/S0169-555X(00)00022-2).
- Hung, O., Leroueil, S., Picarelli, L., 2014. The Varnes classification of landslide types, an update. *Landslides* 11 (2), 167–194. <https://doi.org/10.1007/s10346-013-0436-y>.
- Jalut, G., Belet, J.M., García de Celis, A., Redondo-Vega, J.M., Bonnet, L., Valero-Garcés, B.L., Moreno, A., Villar-Pérez, I., Fontugne, M., Debouat, J.J., González-Sampérez, P., Santos-Hidalgo, I., Vidal-Romani, J.R., 2004. *Reconstrucción paleoambiental de los últimos 35.000 años en el Noroeste de la Península Ibérica: La Laguna de Villaseca (León)*. *Geotemas* 6, 105–109.
- Jalut, G., Turu i Michels, V., Dedouat, J.J., Otto, T., Ezquerro, J., Fontugne, M., Belet, J.M., Bonnet, L., de Celis, A.G., Redondo-Vega, J.M., Vidal-Romani, J.R., Santos, L., 2010. Palaeoenvironmental studies in NW Iberia (Cantabrian range): vegetation history and synthetic approach of the last deglaciation phases in the western Mediterranean. *Palaeogeogr. Palaeoclimatol. Palaeoecol.* 297, 330–350. <https://doi.org/10.1016/j.palaeo.2010.08.012>.
- Janke, J.R., Regmi, N.R., Giardino, J.R., Vitek, J.D., 2013. 8.17 Rock Glaciers. *Treatise Geomorphol.* 8, 238–273. <https://doi.org/10.1016/B978-0-12-374739-6.00211-6>.
- Janke, J.R., Bellisario, A.C., Ferrando, F.A., 2015. Classification of debris-covered glaciers and rock glaciers in the Andes of Central Chile. *Geomorphology* 241, 98–121. <https://doi.org/10.1016/j.geomorph.2015.03.034>.
- Jiménez-Sánchez, M., Rodríguez-Rodríguez, L., García-Ruiz, J.M., Domínguez-Cuesta, M.J., Fariás, P., Valero-Garcés, B., Moreno, A., Rico, M., Valcárcel, M., 2013. A review of glacial geomorphology and chronology in northern Spain: timing and regional variability during the last glacial cycle. *Geomorphology* 195, 50–64. <https://doi.org/10.1016/j.geomorph.2012.06.009>.
- Jiménez-Sánchez, M., Rodríguez-Rodríguez, L., González-Lemos, S., Domínguez-Cuesta, M.J., 2021. The glaciers in the Redes Natural Park. In: Oliva, M., Palacios, D., Fernández-Fernández, J.M. (Eds.), *Iberia, Land of Glaciers*. Elsevier, pp. 221–235. <https://doi.org/10.1016/B978-0-12-821941-6.00011-6>.
- Johnson, P.G., 1984. Rock Glacier formation by high-magnitude low-frequency slope processes in the Southwest Yukon. *Ann. Assoc. Am. Geogr.* 74, 408–419.
- Johnson, M.D., 1990. Fabric and origin of diamictites in end moraines, Animas River valley, Colorado, U.S.A. *Arct. Alp. Res.* 22, 14–25. <https://doi.org/10.2307/1551717>.
- Jomelli, V., Chapron, E., Favier, V., Rinterknecht, V., Braucher, R., Tournier, N., Gascoin, S., Marti, R., Galop, D., Binet, S., Deschamps-Berger, C., Tissoux, H., Aumaitre, G., Bourliès, D.L., Keddadouche, K., 2020. Glacier fluctuations during the late Glacial and Holocene on the Ariège valley, northern slope of the Pyrenees and reconstructed climatic conditions. *Mediterr. Geosci. Rev.* 2, 37–51. <https://doi.org/10.1007/s42990-020-00018-5>.
- Kellerer-Pirklbauer, A., 2012. The Schmidt-Hammer as a relative age dating tool for rock glacier surfaces. *Quat. Int.* 279–280, 239. <https://doi.org/10.1016/j.quaint.2012.08.546>.
- Kellerer-Pirklbauer, A., Kaufmann, V., 2012. About the relationship between rock glacier velocity and climate parameters in Central Austria. *Aust. J. Earth Sci.* 105, 94–112.
- Kellerer-Pirklbauer, A., Lieb, G.K., Kaufmann, V., 2017. The Dösen rock glacier in Central Austria: a key site for multidisciplinary long-term rock glacier monitoring in the eastern alps. *Aust. J. Earth Sci.* 110. <https://doi.org/10.17738/ajes.2017.0013>.
- Kenner, R., 2019. Geomorphological analysis on the interaction of Alpine glaciers and rock glaciers since the Little Ice Age. *Land Degrad. Dev.* 30, 580–591. <https://doi.org/10.1002/ldr.3238>.
- Kerschner, H., 1978. Paleoclimatic inferences from Late Wurm rock glaciers, eastern central Alps, western Tyrol, Austria. *Arct. Alp. Res.* 10 (3), 635–644. <https://doi.org/10.1080/00040851.1978.12004000>.
- Kirkbride, M.P., 2000. *Ice-marginal Geomorphology and Holocene Expansion of Debris-covered Tasman Glacier, New Zealand*. IAHS-AISH Publication.
- Kjær, K.H., Krüger, J., 1998. Does clast size influence fabric strength? *J. Sediment. Res.* 5, 746–749. <https://doi.org/10.1306/D4268865-2B26-11D7-8648000102C1865D>.
- Knight, J., Harrison, S., Jones, D.B., 2019. Rock glaciers and the geomorphological evolution of deglaciating mountains. *Geomorphology* 324, 14–24. <https://doi.org/10.1016/j.geomorph.2018.09.020>.
- Korschinek, G., Bergmaier, A., Faestermann, T., Gerstmann, U.C., Knie, K., Rugel, G., Wallner, A., Dillmann, I., Dollinger, G., von Gostomski, C.L., Kossert, K., Maiti, M., Poutivsev, M., Remmert, A., 2010. A new value for the half-life of <sup>10</sup>Be by heavy-ion elastic recoil detection and liquid scintillation counting. *Nucl. Instrum. Methods Phys. Res., Sect. B* 268, 187–191. <https://doi.org/10.1016/j.nimb.2009.09.020>.

- Lal, D., 1991. Cosmic ray labeling of erosion surfaces: in situ nuclide production rates and erosion models. *Earth Planet. Sci. Lett.* 104, 424e439. [https://doi.org/10.1016/0012-821X\(91\)90220-C](https://doi.org/10.1016/0012-821X(91)90220-C).
- Li, Y., 2018. Determining topographic shielding from digital elevation models for cosmogenic nuclide analysis: a GIS model for discrete sample sites. *J. Mt. Sci.* 15, 939–947. <https://doi.org/10.1007/s11629-018-4895-4>.
- Linge, H., Nesje, A., Matthews, J.A., Fabel, D., Xu, S., 2020. Evidence for rapid paraglacial formation of rock glaciers in southern Norway from 10Be surface-exposure dating. *Quat. Res.* 97, 55–70. <https://doi.org/10.1017/qua.2020.10>.
- López-Sáez, J.A., Carrasco, R.M., Turu, V., Ruiz-Zapata, B., Gil-García, M.J., Luermo-Lautenschlaeger, R., Pérez-Díaz, S., Alba-Sánchez, F., Abel-Schaad, D., Ros, X., Pedraza, J., 2020. Late Glacial-early holocene vegetation and environmental changes in the western Iberian Central System inferred from a key site: the Navamuño record, Béjar range (Spain). *Quat. Sci. Rev.* 230, 106167. <https://doi.org/10.1016/j.quascirev.2020.106167>.
- Mackay, S.L., Marchant, D.R., 2016. Dating buried glacier ice using cosmogenic <sup>3</sup>He in surface clasts: theory and application to Mullins Glacier, Antarctica. *Quat. Sci. Rev.* 140, 75–100. <https://doi.org/10.1016/j.quascirev.2016.03.013>.
- Marcet, M., Cicoira, A., Cusicanqui, D., Bodin, X., Echelard, T., Obregon, R., Schoeneich, P., 2021. Rock glaciers throughout the French Alps accelerated and destabilised since 1990 as air temperatures increased. *Commun. Earth Environ.* 2 (81), 1–11. <https://doi.org/10.1038/s43247-021-00150-6>.
- Mark, D.M., 1973. Analysis of axial orientation data, including till fabrics. *Bull. Geol. Soc. Am.* 84, 1369–1374. [https://doi.org/10.1130/0016-7606\(1973\)84<1369:AOAODI>2.CO;2](https://doi.org/10.1130/0016-7606(1973)84<1369:AOAODI>2.CO;2).
- Marr, P., Winkler, S., Löffler, J., 2019. Schmidt-hammer exposure-age dating (SHD) performed on periglacial and related landforms in Opplandskedalen, Geirangerfjellet, Norway: implications for mid- and late-Holocene climate variability. *The Holocene* 29, 97–109. <https://doi.org/10.1177/0959683618804634>.
- Martin, L.C.P., Blard, P.-H., Balco, G., Lavé, J., Delunel, R., Lifton, N., Laurent, V., 2017. The CRÉP program and the ICE-D production rate calibration database: a fully parameterizable and updated online tool to compute cosmic-ray exposure ages. *Quat. Geochronol.* 38, 25–49. <https://doi.org/10.1016/j.quageo.2016.11.006>.
- Martín-González, F., Heredia, N., 2011. Geometry, structures and evolution of the western termination of the Alpine-Pyrenean Orogen reliefs (NW Iberian Peninsula). *J. Iber. Geol.* 37, 103–120. [https://doi.org/10.5209/rev\\_JIGE.2011.v37.n2.1](https://doi.org/10.5209/rev_JIGE.2011.v37.n2.1).
- Martrat, B., Jimenez-Amat, P., Zahn, R., Grimalt, J.O., 2014. Similarities and dissimilarities between the last two deglaciations and interglaciations in the North Atlantic region. *Quat. Sci. Rev.* 99, 122–134. <https://doi.org/10.1016/j.quascirev.2014.06.016>.
- Matthews, J.A., Wilson, P., Winkler, S., Mourne, R.W., Hill, J.L., Owen, G., Hiemstra, J.F., Hallang, H., Geary, A.P., 2019. Age and development of active cryoplanation terraces in the alpine permafrost zone at Svartkampan, Jotunheimen, southern Norway. *Quat. Res.* 92, 641–664. <https://doi.org/10.1017/qua.2019.41>.
- Mayr, E., Hagg, W., 2019. Debris-covered Glaciers. In: Heckmann, T., Morche, D. (Eds.), *Geomorphology of Proglacial Systems, Geography of the Physical Environment*, pp. 59–71. [https://doi.org/10.1007/978-3-319-94184-4\\_4](https://doi.org/10.1007/978-3-319-94184-4_4).
- McManus, J.F., Francois, R., Gherardi, J.-M., Keigwin, L.D., Brown-Leger, S., 2004. Collapse and rapid resumption of Atlantic meridional circulation linked to deglacial climate changes. *Nat* 4286985 (428), 834–837. <https://doi.org/10.1038/nature02494>.
- Merchel, S., Herpers, U., 1999. An update on radiochemical separation techniques for the determination of long-lived radionuclides via accelerator mass spectrometry. *Radiochim. Acta* 84, 215–219. <https://doi.org/10.1524/ract.1999.84.4.215>.
- Merchel, S., Arnold, M., Aumaître, G., Benedetti, L., Bourlès, D.L., Braucher, R., Alfimov, V., Freeman, S.P.H.T., Steier, P., Wallner, A., 2008. Nuclear instruments and methods in physics research B towards more precise 10 Be and 36 Cl data from measurements at the 10 Å level: influence of sample preparation by B e. *Nucl. Inst. Methods Phys. Res. B* 266, 4921–4926. <https://doi.org/10.1016/j.nimb.2008.07.031>.
- Monnier, S., Kinnard, C., 2015. Reconsidering the glacier to rock glacier transformation problem: new insights from the Central Andes of Chile. *Geomorphology* 238, 47–55. <https://doi.org/10.1016/j.geomorph.2015.02.025>.
- Monnier, S., Kinnard, C., 2017. Pluri-decadal (1955–2014) evolution of glacier-rock glacier transitional landforms in the Central Andes of Chile (30–33deg;S). *Earth Surf. Dyn.* 5, 493–509. <https://doi.org/10.5194/ESURF-5-493-2017>.
- Moran, A.P., Ivy Ochs, S., Vockenhuber, C., Kerschner, H., 2016. Rock glacier development in the Northern Calcareous Alps at the Pleistocene-Holocene boundary. *Geomorphology* 273, 178–188. <https://doi.org/10.1016/j.geomorph.2016.08.017>.
- Moreno, A., Stoll, H., Jiménez-Sánchez, M., Cacho, I., Valero-Garcés, B., Ito, E., Edwards, R.L., 2010. A speleothem record of glacial (25–11.6 kyr BP) rapid climatic changes from northern Iberian Peninsula. *Glob. Planet. Chang.* 71, 218–231. <https://doi.org/10.1016/j.gloplacha.2009.10.002>.
- Moreno, A., Svensson, A., Brooks, S.J., Connor, S., Engels, S., Fletcher, W., Genty, D., Heiri, O., Labuhn, I., Perşoiu, A., Peyron, O., Sadori, L., Valero-Garcés, B., Wulf, S., Zanchetta, G., Allen, J.R.M., Ampel, L., Blamart, D., Birks, H., Blockley, S., Borsato, A., Bos, H., Brauer, A., Combourieu-Nebout, N., de Beaulieu, J.L., Drescher-Schneider, R., Drysdale, R., Elias, S., Frisia, S., Hellstrom, J.C., Ilyashuk, B., Joannin, S., Kühl, N., Larocque-Tobler, I., Lotter, A., Magny, M., Matthews, I., McDermott, F., Millet, L., Morellón, M., Neugebauer, I., Muñoz-Sobrino, C., Naughton, F., Ohlwein, C., Roucoux, K., Samartin, S., Sánchez-Goni, M.F., Sirocco, F., van Asch, N., van Geel, B., van Grafenstein, U., Vanniëre, B., Vegas, J., Veres, D., Walker, M., Wohlfarth, B., 2014. A compilation of Western European terrestrial records 60–8kaBP: towards an understanding of latitudinal climatic gradients. *Quat. Sci. Rev.* 106, 167–185. <https://doi.org/10.1016/j.quascirev.2014.06.030>.
- Muscheler, R., Beer, J., Kubik, P.W., Synal, H.-A., 2005. Geomagnetic field intensity during the last 60,000 years based on 10Be and 36Cl from the Summit ice cores and 14C. *Quat. Sci. Rev.* 24. <https://doi.org/10.1016/j.quascirev.2005.01.012> 1849e1860.
- Naughton, F., Sanchez Goñi, M.F., Rodrigues, T., Salgueiro, E., Costas, S., Desprat, S., Duprat, J., Michel, E., Rossignol, L., Zaragosi, S., Voelker, A.H.L., Abrantes, F., 2016. Climate variability across the last deglaciation in NW Iberia and its margin. *Quat. Int.* 414, 9–22. <https://doi.org/10.1016/j.quaint.2015.08.073>.
- Niedzielski, T., Migoń, P., Placek, A., 2009. A minimum sample size required from Schmidt hammer measurements. *Earth Surf. Process. Landf.* 34, 1713–1725. <https://doi.org/10.1002/esp.1851>.
- Oliva, M., Žebre, M., Guglielmin, M., Hughes, P.D., Çiner, A., Vieira, G., Bodin, X., Andrés, N., Colucci, R.R., García-Hernández, C., Mora, C., Nofre, J., Palacios, D., Pérez-Alberti, A., Ribolini, A., Ruiz-Fernández, J., Sanjaya, M.A., Serrano, E., Urdea, P., Valcárcel, M., Woodward, J.C., Yildirim, C., 2018. Permafrost conditions in the Mediterranean region since the last Glaciation. *Earth Sci. Rev.* 185, 397–436. <https://doi.org/10.1016/j.earscirev.2018.06.018>.
- Oliva, M., Palacios, D., Fernández-Fernández, J.M., Rodríguez-Rodríguez, L., García-Ruiz, J.M., Andrés, N., Carrasco, R.M., Pedraza, J., Pérez-Alberti, A., Valcárcel, M., Hughes, P.D., 2019. Late Quaternary glacial phases in the Iberian Peninsula. *Earth Sci. Rev.* 192, 564–600. <https://doi.org/10.1016/j.earscirev.2019.03.015>.
- Oliva, M., Fernandes, M., Palacios, D., Fernández-Fernández, J.-M., Schimmelpfennig, I., Antoniades, D., ASTER Team, 2021. Rapid deglaciation during the Bølling-Allerød Interstadial in the Central Pyrenees and associated glacial and periglacial landforms. *Geomorphology* 385, 107735. <https://doi.org/10.1016/j.geomorph.2021.107735>.
- Oniga, V.E., Breaban, A.I., Pfeifer, N., Chirila, C., 2020. Determining the suitable number of ground control points for UAS images georeferencing by varying number and spatial distribution. *Remote Sens.* 12, 876. <https://doi.org/10.3390/rs12050876>.
- Palacios, D., de Andrés, N., de Marcos, J., Vázquez-Selem, L., 2012. Glacial landforms and their paleoclimatic significance in Sierra de Guadarrama, Central Iberian Peninsula. *Geomorphology* 139–140, 67–78. <https://doi.org/10.1016/j.geomorph.2011.10.003>.
- Palacios, D., Gómez-Ortiz, A., Andrés, N., Salvador, F., Oliva, M., 2016. Timing and new geomorphological evidence of the last deglaciation stages in Sierra Nevada (southern Spain). *Quat. Sci. Rev.* 150, 110–129. <https://doi.org/10.1016/j.quascirev.2016.08.012>.
- Palacios, D., García-Ruiz, J.M., Andrés, N., Schimmelpfennig, I., Campos, N., Léanni, L., ASTER Team, 2017. Deglaciation in the central Pyrenees during the Pleistocene-Holocene transition: timing and geomorphological significance. *Quat. Sci. Rev.* 162, 111–127. <https://doi.org/10.1016/j.quascirev.2017.03.007>.
- Palacios, D., Gómez-Ortiz, A., Alcalá-Reygosa, J., Andrés, N., Oliva, M., Tanarro, L.M., Salvador-Franch, F., Schimmelpfennig, I., Fernández-Fernández, J.M., Léanni, L., 2019. The challenging application of cosmogenic dating methods in residual glacial landforms: the case of Sierra Nevada (Spain). *Geomorphology* 325, 103–118. <https://doi.org/10.1016/j.geomorph.2018.10.006>.
- Palacios, D., Oliva, M., Gómez-Ortiz, A., Andrés, N., Fernández-Fernández, J.M., Schimmelpfennig, I., Léanni, L., Team, A.S.T.E.R., 2020. Climate sensitivity and geomorphological response of cirque glaciers from the late glacial to the Holocene, Sierra Nevada, Spain. *Quat. Sci. Rev.* 248, 106617. <https://doi.org/10.1016/j.quascirev.2020.106617>.
- Palacios, D., Rodríguez-Mena, M., Fernández-Fernández, J.M., Schimmelpfennig, I., Tanarro, L.M., Zamorano, J.J., Andrés, N., Úbeda, J., Sæmundsson, P., Brynjólfsson, S., Oliva, M., Team, A., 2021. Reversible glacial-periglacial transition in response to climate changes and paraglacial dynamics: a case study from Hédindsalsjökull (northern Iceland). *Geomorphology* 388, 107787. <https://doi.org/10.1016/j.geomorph.2021.107787>.
- Pellitero, R., 2021. The glaciers of the Montaña Palentina. Iberia, Land of Glaciers. Elsevier, pp. 179–199. <https://doi.org/10.1016/B978-0-12-821941-6.00009-8>.
- Pellitero, R., Serrano, E., González Trueba, J.J., 2011. Rock glaciers in the central cantabrian mountains: palaeoenvironmental indicators. *Cuad. Investig. Geogr.* 37, 119–144. <https://doi.org/10.18172/cig.1259>.
- Pérez-Alberti, A., Valcárcel, M., 2021. The glaciers in Eastern Galicia. Iberia, Land of Glaciers. Elsevier, pp. 375–395. <https://doi.org/10.1016/B978-0-12-821941-6.00018-9>.
- Pisabarro, A., Pellitero, R., Serrano, E., Gómez-Lende, M., González-Trueba, J.J., 2017. Ground temperatures, landforms and processes in an Atlantic mountain. *Cantabrian Mountains (Northern Spain)*. *Catena* 149, 623–636. <https://doi.org/10.1016/j.catena.2016.07.051>.
- Rasmussen, S.O., Bigler, M., Blockley, S.P., Blunier, T., Buchardt, S.L., Clausen, H.B., Cvijanovic, I., Dahl-Jensen, D., Johnsen, S.J., Fischer, H., Gkinis, V., Guillevic, M., Hoek, W.Z., Lowe, J.J., Pedro, J.B., Popp, T., Seierstad, I.K., Steffensen, J.P., Svensson, A.M., Vallelonga, P., Vinther, B.M., Walker, M.J.C., Wheatley, J.J., Winstrup, M., 2014. A stratigraphic framework for abrupt climatic changes during the last Glacial period based on three synchronized Greenland ice-core records: refining and extending the INTIMATE event stratigraphy. *Quat. Sci. Rev.* 106, 14–28. <https://doi.org/10.1016/j.quascirev.2014.09.007>.
- Redondo-Vega, J.M., Gómez-Villar, A., González-Gutiérrez, R.B., 2004. Localización y caracterización morfológica de los glaciares rocosos relictos de la Sierra de Gistredo (Montaña Cantábrica, León). *Cuad. Investig. Geogr.* 30, 35–60. <https://doi.org/10.18172/cig.1134>.
- Redondo-Vega, J.M., Gómez-Villar, A., González-Gutiérrez, R.B., Santos-González, J., 2010. *Los glaciares rocosos de la Cordillera Cantábrica*. Universidad de León, León.
- Renssen, H., Sepå, H., Crosta, X., Gooose, H., Roche, D.M., 2012. Global characterization of the Holocene thermal maximum. *Quat. Sci. Rev.* 48, 7–19. <https://doi.org/10.1016/j.quascirev.2012.05.022>.
- RGIK, 2021. IPA Action Group Rock glacier inventories and kinematics. Towards standard guidelines for inventorying rock glaciers. <https://www.unifir.ch/geo/geomorphology/en/research/>.
- Rodrigo-Gámiz, M., Martínez-Ruiz, F., Rampen, S.W., Schouten, S., Damsté, J.S.S., 2014. Sea surface temperature variations in the western Mediterranean Sea over the last 20 kyr: a dual-organic proxy (UK'37 and LDI) approach. *Paleoceanography* 29, 87–98. <https://doi.org/10.1002/2013PA002466>.

- Rodríguez, A., Suárez, A., Alonso, V., 2020. Los glaciares rocosos del Valle de Lumajo (Cordillera Cantábrica). *Geogaceta* 68, 59–62.
- Rodríguez-Rodríguez, L., Jiménez-Sánchez, M., Domínguez-Cuesta, M.J., Aranburu, A., 2015. Research history on glacial geomorphology and geochronology of the Cantabrian Mountains, North Iberia (43–42°N/7–2°W). *Quat. Int.* 364, 6–21. <https://doi.org/10.1016/j.quaint.2014.06.007>.
- Rodríguez-Rodríguez, L., Jiménez-Sánchez, M., Domínguez-Cuesta, M.J., Rinterknecht, V., Pallàs, R., Bourlès, D., 2016. Chronology of glaciations in the Cantabrian Mountains (NW Iberia) during the last Glacial Cycle based on in situ-produced  $^{10}\text{Be}$ . *Quat. Sci. Rev.* 138, 31–48. <https://doi.org/10.1016/j.quascirev.2016.02.027>.
- Rodríguez-Rodríguez, L., Jiménez-Sánchez, M., Domínguez-Cuesta, M.J., Rinterknecht, V., Pallàs, R., ASTER Team, 2017. Timing of last deglaciation in the Cantabrian Mountains (Iberian Peninsula; North Atlantic Region) based on in situ-produced  $^{10}\text{Be}$  exposure dating. *Quat. Sci. Rev.* 171, 166–181. <https://doi.org/10.1016/j.quascirev.2017.07.012>.
- Rodríguez-Rodríguez, L., Jiménez-Sánchez, M., Domínguez-Cuesta, M.J., González-Lemos, S., 2021. The glaciers around Lake Sanabria. In: Oliva, M., Palacios, D., Fernández-Fernández, J.M. (Eds.), *Iberia, Land of Glaciers*. Elsevier, pp. 335–351. <https://doi.org/10.1016/B978-0-12-821941-6.00016-5>.
- Ruiz-Fernández, J., Oliva, M., Cruces, A., Lopes, V., Freitas, M. da C., Andrade, C., García-Hernández, C., López-Sáez, J.A., Gerales, M., 2016. Environmental evolution in the Picos de Europa (Cantabrian Mountains, SW Europe) since the Last Glaciation. *Quat. Sci. Rev.* 138, 87–104. <https://doi.org/10.1016/j.quascirev.2016.03.002>.
- Ruiz-Fernández, J., García-Hernández, C., Gallinar-Cañedo, D., 2021a. The glaciers of the Picos de Europa. In: Oliva, M., Palacios, D., Fernández-Fernández, J.M. (Eds.), *Iberia, Land of Glaciers*. Elsevier, pp. 237–263. <https://doi.org/10.1016/B978-0-12-821941-6.00012-8>.
- Ruiz-Fernández, J., González-Díaz, B., Gallinar-Cañedo, D., García-Hernández, C., 2021b. The glaciers of the Central-Western Asturian Mountains. In: Oliva, M., Palacios, D., Fernández-Fernández, J.M. (Eds.), *Iberia, Land of Glaciers*. Elsevier, pp. 265–288. <https://doi.org/10.1016/B978-0-12-821941-6.00013-X>.
- Santos-González, J., Redondo-Vega, J.M., 2006. *Geología, Geomorfología, Suelos e Hidrología*. DirIn: Redondo-Vega, J.M. (Ed.), *Diagnosís Territorial y Bases Para La Ordenación, El Uso y La Gestión Del Alto Sil (León)* Unpublished.
- Santos-González, J., Redondo-Vega, J.M., González-Gutiérrez, R.B., Gómez-Villar, A., 2013a. Applying the AABR method to reconstruct equilibrium-line altitudes from the last glacial maximum in the Cantabrian Mountains (SW Europe). *Palaeogeogr. Palaeoclimatol. Palaeoecol.* 387, 185–199. <https://doi.org/10.1016/j.palaeo.2013.07.025>.
- Santos-González, J., Santos, J.A., González-Gutiérrez, R.B., Redondo-Vega, J.M., Gómez-Villar, A., 2013b. Till fabric and grain-size analysis of glacial sequences in the Upper Sil River Basin, Cantabrian Mountains, NW Spain. *Phys. Geogr.* 34, 471–490. <https://doi.org/10.1080/02723646.2013.855989>.
- Santos-González, J., González-Gutiérrez, R.B., Santos, J.A., Gómez-Villar, A., Peña-Pérez, S.A., Redondo-Vega, J.M., 2018. Topographic, lithologic and glaciation style influences on paraglacial processes in the upper Sil and Luna catchments, Cantabrian Mountains, NW Spain. *Geomorphology* 319, 133–146. <https://doi.org/10.1016/j.geomorph.2018.07.019>.
- Santos-González, J., Redondo-Vega, J.M., García-de Celis, A., Blanca González-Gutiérrez, R., Gómez-Villar, A., 2021. The glaciers of the Leonese Cantabrian Mountains. In: Oliva, M., Palacios, D., Fernández-Fernández, J.M. (Eds.), *Iberia, Land of Glaciers*. Elsevier, pp. 289–314. <https://doi.org/10.1016/B978-0-12-821941-6.00014-1>.
- Scherler, D., Egholm, D.L., 2020. Production and transport of Supraglacial debris: insights from Cosmogenic  $^{10}\text{Be}$  and numerical modeling, Chhota Shigri Glacier, Indian Himalaya. *J. Geophys. Res. Earth Surf.* 125, e2020JF005586.
- Serrano, E., González-Trueba, J.J., Santos, J.J., Del Rio, L.M., 2011. Ice patch origin, evolution and dynamics in a temperate high mountain environment: the Jou Negro, Picos de Europa (NW Spain). *Geogr. Ann., Ser. A* 93 (2), 57–70. <https://doi.org/10.1111/j.1468-0459.2011.00006.x>.
- Serrano, E., González-Trueba, J.J., Pellitero, R., González-García, M., Gómez-Lende, M., 2013. Quaternary glacial evolution in the Central Cantabrian Mountains (Northern Spain). *Geomorphology* 196, 65–82. <https://doi.org/10.1016/j.geomorph.2012.05.001>.
- Serrano, E., Gómez-Lende, M., Pellitero, R., González Trueba, J.J., 2015. Deglaciation in the Cantabrian Mountains: pattern and evolution. *Cuad. Investig. Geogr.* 41, 389. <https://doi.org/10.18172/cig.2716>.
- Serrano, E., González-Trueba, J.J., Pellitero, R., Gómez-Lende, M., 2017. Quaternary glacial history of the Cantabrian Mountains of northern Spain: a new synthesis. *Geol. Soc. Spec. Pub.*, 55–85. <https://doi.org/10.1144/SP433.8>.
- Serrano, E., Gómez-Lende, M., González-Amuchastegui, M.J., 2021a. The glaciers of the eastern massifs of Cantabria, the Burgos Mountain and the Basque Country. In: Oliva, M., Palacios, D., Fernández-Fernández, J.M. (Eds.), *Iberia, Land of Glaciers*. Elsevier, pp. 157–178. <https://doi.org/10.1016/B978-0-12-821941-6.00008-6>.
- Serrano, E., Gómez-Lende, M., Pisabarro, A., 2021b. The glaciers of the western massifs of Cantabria. In: Oliva, M., Palacios, D., Fernández-Fernández, J.M. (Eds.), *Iberia, Land of Glaciers*. Elsevier, pp. 201–219. <https://doi.org/10.1016/B978-0-12-821941-6.00010-4>.
- Steinmann, O., Reiter, J.M., Ivy-Ochs, S., Christl, M., Synal, H.A., 2020. Tracking rockglacier evolution in the Eastern Alps from the Lateglacial to the early Holocene. *Quat. Sci. Rev.* 241, 106424. <https://doi.org/10.1016/j.quascirev.2020.106424>.
- Stone, J.O., 2000. Air pressure and cosmogenic isotope production. *J. Geophys. Res.* 105, 23753. <https://doi.org/10.1029/2000JB900181>.
- Štroner, M., Urban, R., Reindl, T., Seidl, J., Brouček, J., 2020. Evaluation of the georeferencing accuracy of a photogrammetric model using a quadcopter with onboard GNSS RTK. *Sensors* 20, 2318. <https://doi.org/10.3390/s20082318>.
- Tanarro, L.M., Palacios, D., Andrés, N., Fernández-Fernández, J.M., Zamorano, J.J., Sæmundsson, Þ., Brynjólfsson, S., 2019. Unchanged surface morphology in debris-covered glaciers and rock glaciers in Tröllaskagi peninsula (northern Iceland). *Sci. Total Environ.* 648, 218–235. <https://doi.org/10.1016/j.scitotenv.2018.07.460>.
- Tanarro, L.M., Palacios, D., Fernández-Fernández, J.M., Andrés, N., Oliva, M., Rodríguez-Mena, M., Schimmelpfennig, I., Brynjólfsson, S., Zamorano, J.J., Ubeda, J., Sæmundsson, Þ., ASTER Team, 2021. Origins of the divergent evolution of mountain glaciers during deglaciation: Hofsdalur cirques, Northern Iceland. *Quat. Sci. Rev.* 273, 107248. <https://doi.org/10.1016/j.quascirev.2021.107248>.
- Tomkins, M.D., Dortch, J.M., Hughes, P.D., 2016. Schmidt Hammer exposure dating (SHED): Establishment and implications for the retreat of the last British Ice Sheet. *Quat. Geochronol.* 33, 46–60. <https://doi.org/10.1016/j.quageo.2016.02.002>.
- Tomkins, M.D., Dortch, J.M., Hughes, P.D., Huck, J.J., Stimson, A.G., Delmas, M., Calvet, M., Pallàs, R., 2018a. Rapid age assessment of glacial landforms in the Pyrenees using Schmidt hammer exposure dating (SHED). *Quat. Res.* 90, 26–37. <https://doi.org/10.1017/qua.2018.12>.
- Tomkins, M.D., Huck, J.J., Dortch, J.M., Hughes, P.D., Kirbride, M.P., Barr, I.D., 2018b. Schmidt Hammer exposure dating (SHED): Calibration procedures, new exposure age data and an online calculator. *Quat. Geochronol.* 44, 55–62. <https://doi.org/10.1016/j.quageo.2017.12.003>.
- Tomkins, M.D., Dortch, J.M., Hughes, P.D., Huck, J.J., Pallàs, R., Rodés, Á., Allard, J.L., Stimson, A.G., Bourlès, D., Rinterknecht, V., Jomelli, V., Rodríguez-Rodríguez, L., Copons, R., Barr, I.E., Darvill, C.M., Bishop, T., 2021. *Moraine crest or slope: an analysis of the effects of boulder position on cosmogenic exposure age*. *Earth Planet. Sci. Lett.* 570, 117092.
- Uppala, S.M., Kållberg, P.W., Simmons, A.J., Andrae, U., da Costa Bechtold, V., Fiorino, M., Gibson, J.K., Haseler, J., Hernandez, A., Kelly, G.A., Li, X., Onogi, K., Saarinen, S., Sokka, N., Allan, R.P., Andersson, E., Arpe, K., Balmaseda, M.A., Beljaars, A.C.M., van de Berg, L., Bidlot, J., Bormann, N., Caires, S., Chevallier, F., Dethof, A., Dragosavac, M., Fisher, M., Fuentes, M., Hagemann, S., Hólm, E., Hoskins, B.J., Isaksen, I., Janssen, P.A.E.M., Jenne, R., McNally, A.P., Mahfouf, J.F., Morcrette, J.J., Rayner, N.A., Saunders, R.W., Simon, P., Sterl, A., Trenberth, K.E., Untch, A., Vasiljevic, D., Viterbo, P., Woollen, J., 2005. The ERA-40 re-analysis. *Q. J. R. Meteorol. Soc.* 131, 2961–3012. <https://doi.org/10.1256/qj.04.176>.
- Valet, J.P., Meynadier, L., Guyodo, Y., 2005. Geomagnetic dipole strength and reversal rate over the past two million years. *Nature* 435. <https://doi.org/10.1038/nature03674> 802e805.
- Vidal Box, C., 1958. Algunos datos sobre morfología y depósitos cuaternarios de la región montañosa de Laceda y Babia Alta (provincia de León). *Boletín la Real Soc. Esp. Hist. Nat.* 61, 143–168.
- Vollmer, F.W., 1995. C program for automatic contouring of spherical orientation data using a modified Kamb method. *Comput. Geosci.* 21, 31–49. [https://doi.org/10.1016/0098-3004\(94\)00058-3](https://doi.org/10.1016/0098-3004(94)00058-3).
- Vollmer, F.W., 2015. Orient 3: A new integrated software program for orientation data analysis, kinematic analysis, spherical projections, and Schmidt plots. *Abstr. with Programs - Geol. Soc. Am.*
- Ward, G.K., Wilson, S.R., 1978. Procedures for comparing and combining radiocarbon age determinations: a critique. *Archaeometry* 20, 19–31. <https://doi.org/10.1111/j.1475-4754.1978.tb00208.x>.
- Watson, G.S., 1966. The statistics of orientation data. *J. Geol.* 74, 2. <https://doi.org/10.1086/627211>.
- Westoby, M.J., Brasington, J., Glasser, N.F., Hambrey, M.J., Reynolds, J.M., 2012. “Structure-from-Motion” photogrammetry: a low-cost, effective tool for geoscience applications. *Geomorphology* 179, 300–314. <https://doi.org/10.1016/j.geomorph.2012.08.021>.
- Wilson, P., Matthews, J.A., Mourné, R.W., Linge, H., Olsen, J., 2020. Interpretation, age and significance of a relict paraglacial and periglacial boulder-dominated landform assemblage in Alnesdalen, Romsdalsalpane, southern Norway. *Geomorphology* 369, 107362. <https://doi.org/10.1016/j.geomorph.2020.107362>.
- Winkler, S., Lambiel, C., 2018. Age constraints of rock glaciers in the Southern Alps/New Zealand – exploring their palaeoclimatic potential. *The Holocene* 28, 778–790. <https://doi.org/10.1177/0959683618756802>.
- Winkler, S., Matthews, J.A., Haselberger, S., Hill, J.L., Mourné, R.W., Owen, G., Wilson, P., 2020. Schmidt-hammer exposure-age dating (SHD) of sorted stripes on Juvfyle, Jotunheimen (central South Norway): morphodynamic and palaeoclimatic implications. *Geomorphology* 353, 107014. <https://doi.org/10.1016/j.geomorph.2019.107014>.
- Wirz, V., Gruber, S., Purves, R.S., Beutel, J., Gärtner-Roer, I., Gubler, S., Vieli, A., 2016. Short-term velocity variations at three rock glaciers and their relationship with meteorological conditions. *Earth Surf. Dyn.* 4, 103–123. <https://doi.org/10.5194/esurf-4-103-2016>.
- Woodcock, N.H., 1977. Specification of fabric shapes using an eigenvalue method. *Bull. Geol. Soc. Am.* 88, 1231–1236. [https://doi.org/10.1130/0016-7606\(1977\)88<1231:SOFSUA>2.0.CO;2](https://doi.org/10.1130/0016-7606(1977)88<1231:SOFSUA>2.0.CO;2).